

**Detection of Nitric Oxide using
Carbon Nanotube Field-Effect Transistors**

By

Oleksandr Kuzmych

BS, Kiev State University, 2002

MS, Kiev State University, 2003

Submitted to the Graduate Faculty of
Arts and Sciences in partial fulfillment
of the requirements of MS in Chemistry

University of Pittsburgh

March 2007

UNIVERSITY OF PITTSBURGH

ARTS AND SCIENCES

This dissertation was presented

by

Oleksandr Kuzmych

It was defended on

January 11, 2007

and approved by

Alexander Star, PhD, Assistant Professor

Shigeru Amemiya, PhD, Assistant Professor

Toby Chapman, PhD, Associate Professor

Dissertation Director: Alexander Star, PhD, Assistant Professor

Copyright © by Oleksandr Kuzmych

2007

iii

Detection of Nitric Oxide using Carbon Nanotube Field-Effect Transistors

Oleksandr Kuzmych, M.S.

University of Pittsburgh, 2007

A new method for detection of nitric oxide in gas phase is based on a combination of catalytic conversion and conductivity measurements using a chemically functionalized carbon nanotube field-effect transistor (NTFET) device. Gas mixtures containing nitric oxide (NO) are passed through a catalytic converter (CrO_3), which converts NO into nitrogen dioxide (NO_2). The latter is delivered to the surface of the NTFET sensor coated with poly(ethylene imine) (PEI).

Interaction of the gas with a chemically functionalized NTFET results in a conductivity change that is proportional to the NO gas concentration. The wide range of NO gas concentrations from approximately 2 ppb to 5 ppm was tested. The detection limit of NO has been measured as 5 ppb (S/N=3) in inert atmosphere at a fixed relative humidity (30%).

Cross sensitivity to carbon dioxide and oxygen was measured in the gas mixture, modeling human breath conditions. If CO_2 is removed by means of an ascarite trap, the new method offers the advantage of low cost, compact size and simplicity of set up.

TABLE OF CONTENTS

<u>PART I. Nitric Oxide Detection in Human Breath</u>	1
1. Background.....	1
1.1 Role of Nitric Oxide in Lungs	2
1.2 Physical and Chemical Properties of Nitric Oxide	2
1.3 Methods of Detection of Nitric Oxide	3
1.4 Electrochemical Detection of Nitric Oxide.....	4
1.5 Gas Detection Using Carbon Nanotubes	7
1.6 Principles of Field-Effect Transistor Operation	8
1.7 Carbon Nanotube Field-Effect Transistor (NTFET).....	9
2. Experimental Section.....	12
2.1 Reagents.....	12
2.2 NO Catalytic Conversion.....	13
2.3 Chip Surface Polymer Functionalization	14
3. Results and Discussion	15
3.1 Sensor Dynamic Range.....	19
3.2 Cross Sensitivity to Main Breath Components.....	22
4. Conclusions.....	22
5. Acknowledgments.....	24
<u>PART II. Interactions of Carbon Nanotubes with Metalloporphyrins</u>	25
<u>PART III. Adsorption and Geometry of the Chemisorbed Benzoate Species</u> <u>on Cu(110)</u>	30

<u>Introduction.....</u>	<u>30</u>
<u>Experimental.....</u>	<u>31</u>
<u>Results and Discussion</u>	<u>35</u>
<u>Summary</u>	<u>42</u>
<u>Acknowledgment.....</u>	<u>44</u>
<u>Appendix A. Nitrogen Oxides (NO_x) Chemistry Overview.....</u>	<u>45</u>
<u>Appendix B. Chromium Trioxide Catalyst Chemistry Overview.....</u>	<u>50</u>
<u>References.....</u>	<u>52</u>

LIST OF FIGURES

Figure 1. Architecture of Metal-Oxide-Semiconductor Field-Effect Transistor (MOSFET).....	9
Figure 2. Schematic drawing of carbon nanotube field transistor (NTFET)	10
Figure 3. SEM picture of Si die containing 10 NTFET devices (Nanomix, Inc)	11
Figure 4. Schematic diagram of gas detection setup.....	12
Figure 5. Schematic drawing of polymer coated NTFET device	13
Figure 6. Poly(ethyleneimine) chemical structure	14
Figure 7. Response of bare NTFET to gases	16
Figure 8. Source-drain conductance and SEM photo	18
Figure 9. Dynamic range of NO sensor based on bare and polymer coated NTFET devices	19
Figure 10. Calibration curve of PEI coated sensor in ppbv range	21
Figure 11. Conductance versus time dependence of PEI coated NTFET device	23
Figure 12. Thin film UV-Vis-NIR absorption spectra and conductance versus gate voltage characteristics.....	29
Figure 13. Development of the C(KLL) Auger feature versus exposure to benzoic acid from the heated doser source.....	33
Figure 14. Study of the effect of electron bombardment on the C(KLL) Auger intensity	34
Figure 15. Thermal desorption of benzoic acid from Cu(110).....	36

Figure 16. Development of H⁺- ESDIAD patterns	38
Figure 17. H⁺ ESDIAD patterns for benzoate on Cu(110).....	40
Figure 18. Measured H⁺ polar emission angle for the 3- and 5-positions of the chemisorbed benzoate species on Cu(110)	41
Figure 19. Structure of the chemisorbed benzoate species on Cu(110).....	43
Figure 20. Color of chromium oxide catalyst depending on dominant state of oxidation.....	50

PART I

NITRIC OXIDE GAS DETECTION IN HUMAN BREATH

1. Background

Nitric oxide (NO), an evanescent gas, present in the atmosphere for a long time has been of great environmental concern to scientific community. Produced by car exhausts, it destroys ozone layer and is involved in acid rain chemistry. However, it has recently been discovered to be an important biological mediator in animals and humans. Nitric oxide plays an extremely important role in lung function. It is formed in lungs of mammals and can be detected in an exhaled air, as was first shown^[1] by Gustafsson *et al.*

Pulmonary NO, for which the endothelium and nerves are the main source, is involved in regulation of diameter of blood vessels, in neurotransmission and immunity mediation. Different structural and inflammatory cells, such as eosinophils, epithelial cells and macrophages, however, produce NO for inflammatory response. Epithelial generated NO, which is relevant to asthma, has been suggested^[2] as a physiological defense against infection and could influence airway disease by its antimicrobial activity. There is a consensus among scientific community that exhaled NO level is markedly elevated in patients with asthma.^[3] In US only asthma is responsible for half a million of hospitalizations and 5,500 deaths per year.^[3] Therefore, a reliable, fast and inexpensive method of NO detection in clinical conditions is desired.

1.1 Role of Nitric Oxide in Lungs

In the lungs NO is involved in regulation of diameter of blood vessels, in neurotransmission, as an agent of inflammation and immunity mediator. It is also involved in the process of regulation of bacteria growth. The endothelium and nerves are the main source of NO in the lung. However, it is also produced in different structural and inflammatory cells. The latter ones involved in asthma such as eosinophils, epithelial cells and macrophages. Epithelial generated NO, which is relevant to asthma,^[4] has been suggested as a physiological defense against infection and could influence airway disease by its antimicrobial activity.

1.2 Physical and Chemical Properties of Nitric Oxide

Chemistry of nitrogen oxides (NO_x) is summarized in Appendix A.

At room temperature nitric oxide is a colorless gas, which in the absence of oxygen dissolves in water. It's stable at low concentrations. As it contains an odd number of electrons it's considered a free radical having paramagnetic properties. Thus it can react with a number of atoms and free radicals. NO is oxidized by O₂ to form nitrites and nitrates. Superoxide anion forms peroxinitrite anion with NO, which reacts with biomolecules *in vivo* causing their nitrosation and peroxidation. Nitric oxide has a large affinity towards Fe²⁺ moiety of haemoproteins forming nitrosyl products. It is 3,000

times higher than that for oxygen.^[5] This property may be used for its measurement, taking into account shifts in the absorption spectra. Upon reaction with ozone nitric oxide generates a chemiluminescent product; hence another method of detection is possible. Diazotization of sulfanilic acid at $\text{pH} < 7$ is catalyzed by NO, which can be used for *in vivo* measurements. Nitric oxide is synthesized in cells by oxidation of L-arginine to NO and L-citrulline. The reaction is catalyzed by enzymes.

1.3 Methods of Detection of Nitric Oxide

Several classical methods for detection of nitric oxide, which are the most widely used, are described below.

Amperometric detection is based on the fact that NO gas is readily oxidized when a pair of electrodes consisting of working and reference (usually Ag/AgCl) is immersed into a sample NO solution and a positive potential of 0.9 V is applied. NO is oxidized at the working electrode surface resulting in the generation of a small redox current. Nitrite is a final product of oxidation reaction and redox current is proportional to NO concentration in a solution.^[6]

Gas phase chemiluminescence detection of NO was developed in early 1970s for environmental monitoring. The technique is based on the reaction of NO with ozone (O_3) to produce nitrogen dioxide in the excited state. As excitation quenches, a red photon is emitted which can be detected by photomultiplier with a cutoff filter.^[7]

Fluorometric methods are very useful in bioimaging of NO.^[8] The fluorescence reagents mostly employ adjacent amino groups and exploit the ability of NO to produce N-nitrosating agents to form triazols. For example, 2,3-diaminonaphthalene (DAN) may be used as a fluorescent indicator of NO formation. DAN itself has a weak fluorescence signal but in the presence of NO its intensity increases more than 100 times (λ_{em} = 415 nm). The detection limit of this method is below 50 nM.

An example of diode laser measurement technique for NO detection was proposed by B.Oh.^[9] An antimonide laser operating at 2.65 μm was used to measure absorption lines of NO in the first overtone band. An absorption feature was chosen so it does not interfere with water, thus selective detection of NO became possible. The corresponding detection sensitivity of this method in air at reduced pressure is around 15 ppm with a signal to noise ratio of 2.

1.4 Electrochemical Detection of Nitric Oxide

This simple and inexpensive method is widely used and was chosen as a reference technique for comparison with carbon nanotube gas detection. Electrochemical measurement offers a number of benefits: a) selectivity and specificity, resulting from applied potential; b) selectivity resulting from the choice of electrode material; c) high sensitivity and low detection limit; d) possibility of real time measurement; and e) small device size. Voltammetric and amperometric NO detection is currently the only sensitive method to satisfy real time requirements, for analysis of different biological materials. As electrode processes are surface-dependent, the chemical information is directly

converted into an electric signal. If the signal generated is linearly proportional to the concentration of a detected species, it can be used as analytical signal. Differential pulse voltammetry is used in characterizing the properties of chemically modified electrodes toward NO oxidation and in kinetics studies. Its use in biological applications, however, is limited due to strong loss of signal in the background.^[7]

In amperometry, both electrochemical oxidation and reduction can be used for detection of NO. Carbon and noble metals are the most popular choices for working electrode materials,^[10] whereas Ag/AgCl may be used as a reference electrode. Some organic species (L-arginine, dopamine, uric acid) as well as nitrite ion (one of the products of NO oxidation) strongly interfere with NO detection due to similar oxidation potential. In case of electro reductive detection of NO, with N₂O and N₂ being main products, oxygen appears to be the main factor of interference, since its reduction is thermodynamically more favorable. Low sensitivity and strong pH dependence render this method less popular overall.

For abovementioned reasons and in order to enhance selectivity and sensitivity, electrodes are usually modified by polymers with specific properties such as: redox, electronic conductivity and ion exchange. It involves immobilization of chemical microstructure on a host electrode surface to perform a specific task: acceleration of electron-transfer reactions, preferential accumulation or selective membrane permeation.^[11] Moreover, several films of polymers can be combined on the same electrode to perform a specific task. One of the most widely used methods for modifying electrode surface by polymer films has been electrochemical polymerization of a chosen monomer. Galvanostatic, potentiostatic or cyclic voltammetry techniques are suitable for

this task. Three main practical approaches in NO sensor design can be summarized as followed: 1) Clark's type of a sensor with a gas permeable membrane such as chloroprene, nitrocellulose or silicon rubber; 2) direct coating of Nafion and cellulose on electrode surface or combination of NO-selective membrane and non-conducting polymer-modified electrode; 3) electrocatalytical oxidation of NO by modified layer such as IrO₂, palladium modified electrode or metalloporphyrin modified electrode.^[2] The major advantage of using amperometry is its short response time and ability to detect NO before it is consumed by other species. In general, electrochemical NO sensors offer a detection limit in the vicinity of 1nM and a linear range up to 25 μM, depending on sensor used.

To summarize, a number of chemical and physical methods exist today to measure NO concentration in various systems.^[12] They can be subdivided into electrochemical^[13] and spectroscopic such as tunable laser absorption,^[14,15] chemiluminescence,^[16] fluorescence^[17] and ESR.^[18] Most of these methods are not satisfactory for many applications because the systems are too large and complicated for real time *in-vivo* measurement or have low sensitivity. On the other hand, nanotechnology has emerged as a promising tool for gas detection in the concentration range down to 10 parts per trillion (ppt).^[19]

1.5 Gas Detection using Carbon Nanotubes

Carbon nanotubes are hollow cylinders of carbon atoms, which depending on the number of graphite shells can be multi-walled (MWNTs) or single-walled (SWNTs) and can show different symmetry and diameter, which determines their semiconducting and metallic properties. Since their discovery by Iijima in 1991 they have drawn a considerable amount of attention inside the research community.^[20]

Carbon nanotubes are atomically well-defined quasi one-dimensional systems which show unique mechanical, electronic and chemical properties that make them promising candidates for nanometer-scale electronic devices. In SWNT all carbon atoms are located on the surface where current flows, making a stable conduction channel, which is extremely sensitive to a surrounding chemical environment. From the point of view of sensor technology the most interesting property, however, is the ability of semiconducting SWNTs to change their conductance in response to absorption of different gases.^[21] The idea was successfully implemented in the production of SWNT based field-effect transistor (FET) device,^[22] where a semiconducting SWNT is contacted by two metal electrodes representing the source (S) and the drain (D) with a Si back gate separated by a SiO₂ insulating layer in a transistor-configured circuit. Molecules of analyte gas can adsorb on the nanotube channel that is open to the environment. Thus, a change in conductance is monitored versus time or applied gate voltage. In practice, using methods of photolithography and metal deposition, several micron-size interdigitated NTFET devices can be prepared on a single chip, where the conduction channel is a random network of a mixture of semiconducting and metallic nanotubes

grown on a substrate by catalytic chemical vapor deposition (CVD). Being extremely sensitive, such a device, however, lacks selectivity. In order to make a device selective to either NO₂ or NH₃ gases, a method of non-covalent modification of nanotube surface with polymer molecules has been successfully used.^[23] A combination of chemical functional groups which have a strong affinity to electron withdrawing species, such as NO₂ on one polymer with a semi-permeable film on another, renders a truly selective chemical response. In another example a combination of poly(ethyleneimine) PEI and starch on CNFET, the device is sensitive enough to detect from 500 ppm to 10% of CO₂ gas in air.^[24] In order to detect CO₂ gas in human breath, the same approach was used to develop a commercial real-time portable sensor.^[25]

The current invention is based on electronic detection using a carbon nanotube field effect transistor (NTFET) device, which was used for detection of such gases as NH₃, NO₂,^{[26], [27]} CO, CO₂, H₂S,^{[28], [29]} H₂,^[30] CH₄,^[31] and alcohol vapors.^[32]

1.6 Principles of Field-Effect Transistor Operation

A field effect transistor has only two layers of semiconductor material, one on top of the other. Electricity flows through one of the layers, called the channel. A voltage connected to the other layer, called the gate, interferes with the current flowing in the channel. Thus, the voltage connected to the gate controls the strength of the current in the channel (Figure1). Chemical properties of semiconducting material of the channel determine the character of the device: if the dominant current carriers are electrons (n-

doped Ge) it is classified as n-type. In case these are holes, the device is classified as p-type (p-doped Si, oxygen doped carbon nanotubes).

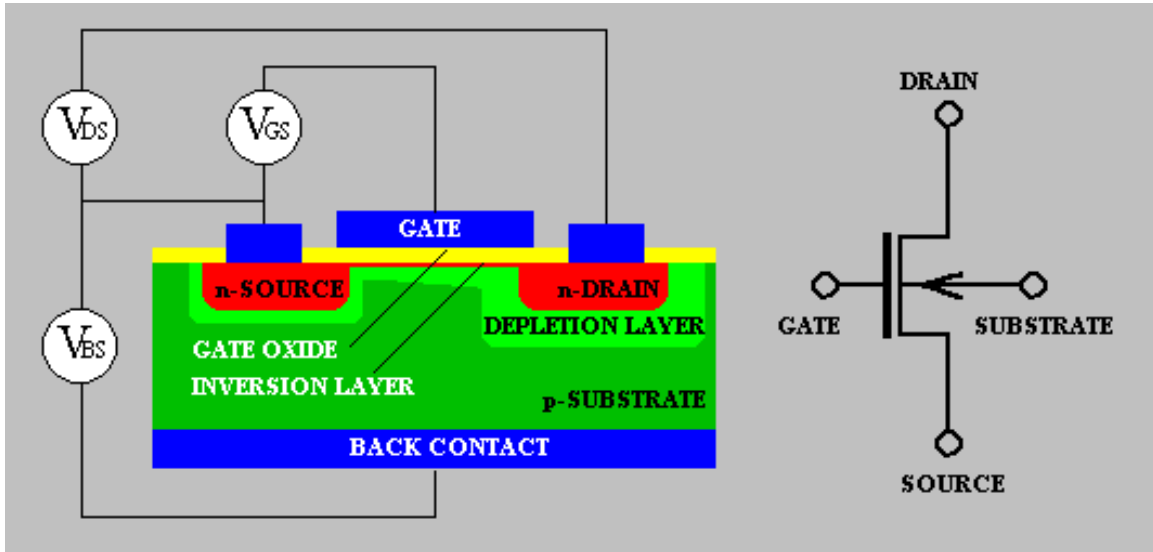


Figure 1. Architecture of Metal-Oxide-Semiconductor Field-Effect Transistor (MOSFET). Depletion layer in between two semiconductor layers creates a conduction channel of the transistor.

1.7 Carbon nanotube field-effect transistor (NTFET) device

In single-walled nanotubes (SWNT) all carbon atoms are located on the surface where current flows, making a stable conduction channel, which is extremely sensitive to a surrounding chemical environment. It has an ability to change its conductance in response to absorption of different gases. This idea is implemented in SWNT based field-effect transistor (FET) device, where a semiconducting SWNT or network of SWNTs is contacted by two metal electrodes representing the source (S) and the drain (D) with a Si back gate separated by a SiO_2 and/or Si_3N_4 insulating layer in a FET-configured circuit (Figure 2). As an analyte comes into contact with the device surface,

SWNT conductance is modified to produce a detection signal. The change in conductance is typically monitored versus time or applied gate voltage.

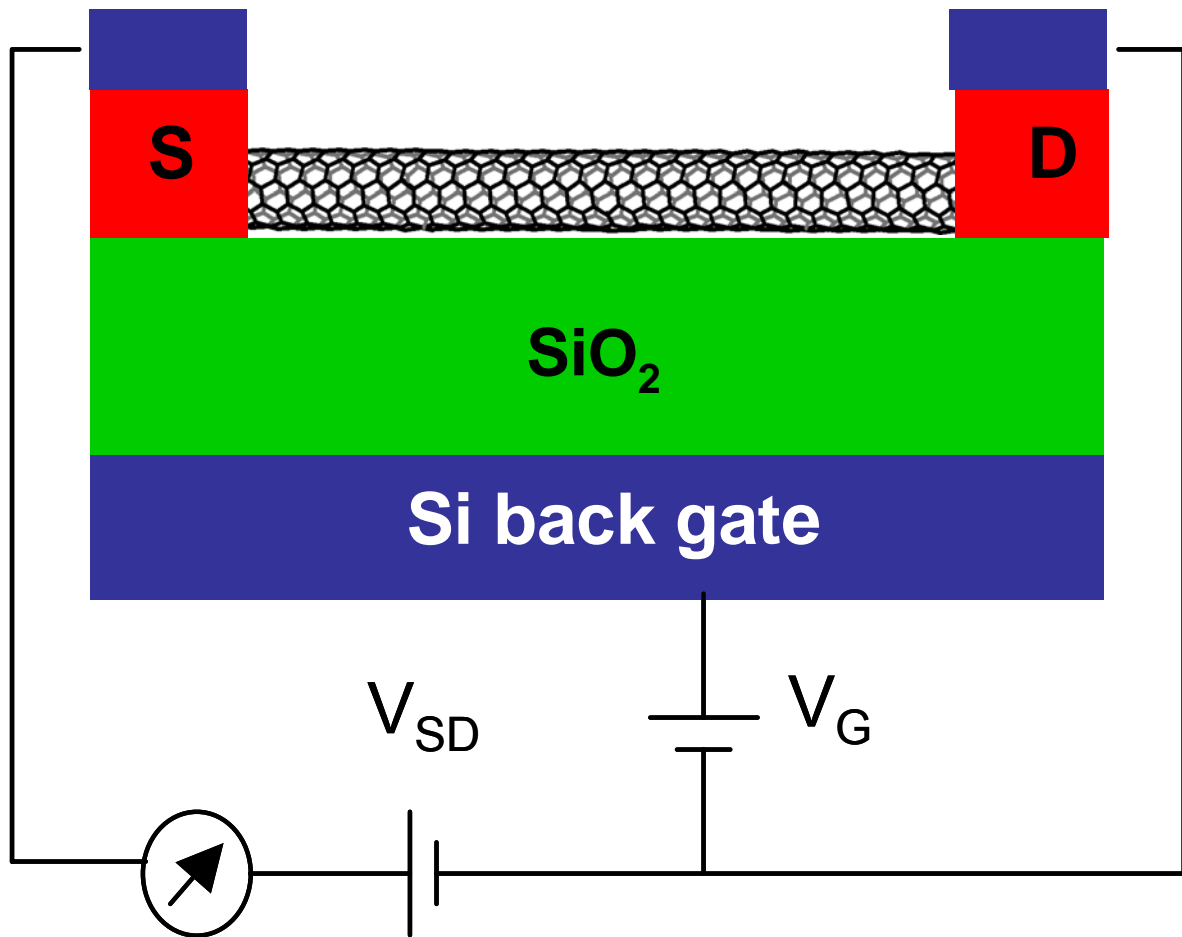


Figure 2. Schematic drawing of carbon nanotube field transistor (NTFET).

For the present work, CNFET devices manufactured by Nanomix Inc., Emeryville, California were used. NTFET devices were prepared using consecutive chemical vapor deposition (CVD) and photolithography process as published elsewhere.^[33] Each Si die containing 10 NTFET devices was mounted on standard Cerdip electronic package with contact pins (Figure 3).

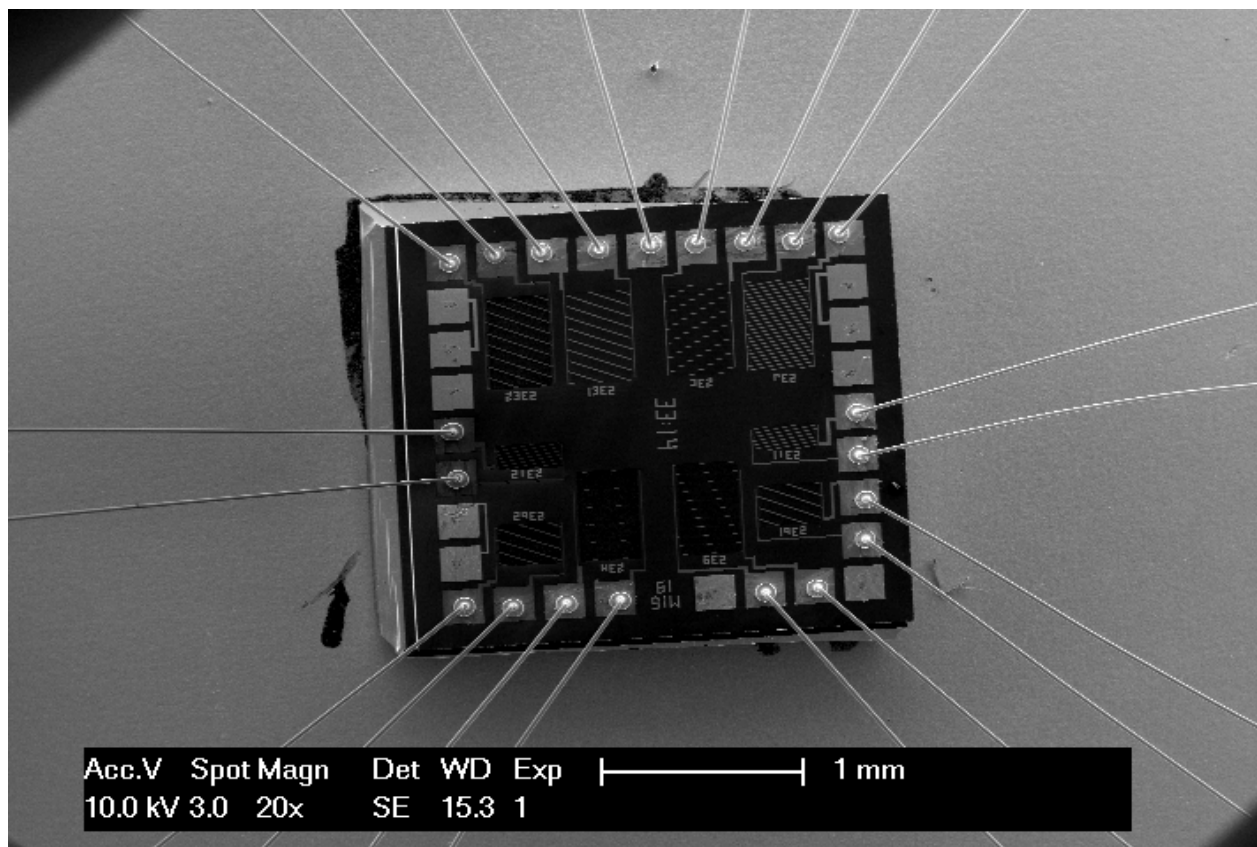


Figure 3. SEM picture of Si die containing 10 NTFET devices (Nanomix, Inc) wire bonded to Cerdip electronic package.

2 EXPERIMENTAL SECTION

2.1 Reagents

Chromium trioxide (CrO_3) (99.98% pure) and 1mm diameter borosilicate glass beads were purchased from Sigma Aldrich, St. Louis, MO. Water-free poly(ethyleneimine) (PEI) with a typical M_w of 25,000 was also obtained from Aldrich.

HPLC grade tetrahydrofuran (THF) was obtained from Spectrum Chemical, CA.

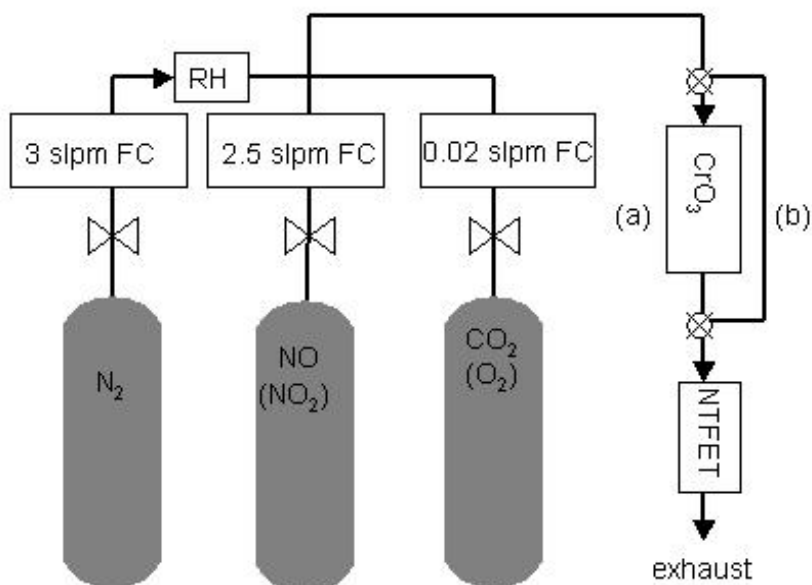


Figure 4. Schematic diagram of gas detection setup. Gas mixtures containing NO and NO_2 gases as well as CO_2 and O_2 contaminants in N_2 environment pass through humidifier to adjust relative humidity (RH). The gas make-up (composition and concentration) is adjusted by three mass-flow controllers (FC). Gas mixtures can pass (a) through catalytic converter (CrO_3) or (b) bypass directly to flow cell containing carbon nanotube field effect transistor (NTFET) device

For drop casting modification of CNFET device $\sim 10^{-3}$ M solution of PEI in THF was used in all cases.

Certified NO and NO₂ gas mixtures in nitrogen with concentrations of 1 ppm (0.92 ppm actual) and 10 ppm, 10% gas mixture of CO₂ in nitrogen, and pure nitrogen and oxygen gases were purchased from National Valley Gases, Inc., PA. High purity dilution N₂ from National Valley Gases, Inc., PA was used for all measurements.

MFC (UNIT Instruments, Inc., MKS, Inc.) were controlled by house built electronics. Relative humidity (RH) of the gas mixtures was adjusted by passing a stream of nitrogen over a saturated salt solution of LiCl in water (15-30% RH) or pure water (>80% RH) (Figure 4). RH and temperature of gas mixture were measured using Sensirion sensor.

2.2 NO Catalytic Conversion

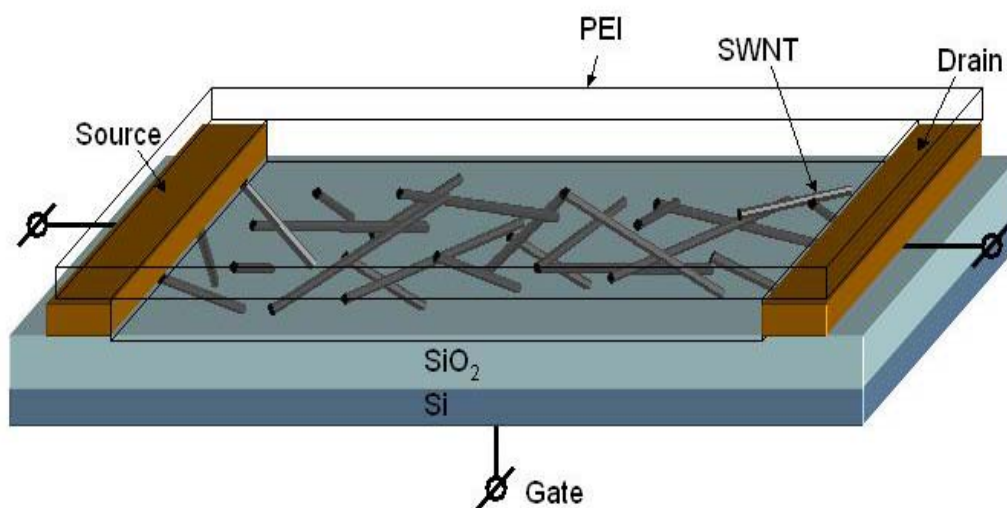


Figure 5. Schematic drawing of polymer coated NTFET device containing random network of SWNTs between gold source and drain electrodes on SiO₂ substrate.

Chromium trioxide (CrO₃) is used as an oxidizing agent to convert nitric oxide (NO) into nitrogen dioxide (NO₂) in a gas phase. (Chemistry of CrO₃ is summarized in Appendix B). Approximately 4g of CrO₃ coated borosilicate glass beads with a diameter of 1mm were packed in a glass tubing 1 cm in diameter and 10 cm in length. Ends of tubing were closed with a glass wool. The coated beads were prepared by immersion into an aqueous solution of CrO₃ in water (1:5 wt) for 30 min. After filtration on a glass filter the beads were dried in a vacuum oven with a temperature of 70°C for two hours.

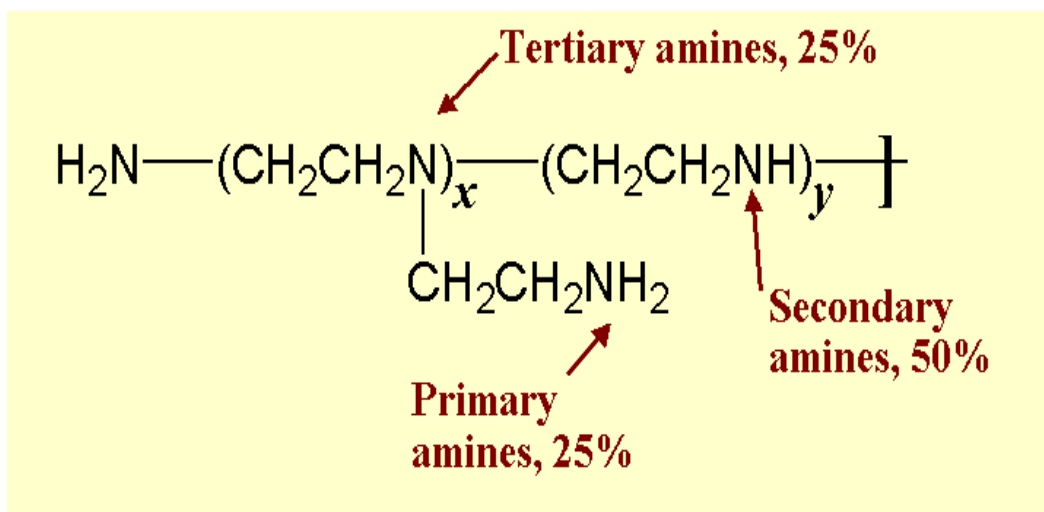


Figure 6. Poly(ethyleneimine) chemical structure.

2.3 Chip Surface Polymer Functionalization

In order to make a device selective to NO₂ gas, surface of the chip was coated with a poly-ethylenimine (PEI) polymer (Figures 5, 6). Branched PEI polymer with an average molecular weight of 25000 kDa was used. A single drop of 10⁻⁴ M solution of PEI in

tetrahydrofuran was drop casted on a CNFET device surface. The device was dried for two hours in the fume- hood at the ambient temperature.

3 RESULTS AND DISCUSSION

The initial response to NO gas pulses (30s) passing over bare carbon nanotubes is shown in Figure 7A. The calculated concentration is around 5 ppm. After initial 500s a flow of gas is switched to the CrO₃ catalytic converter which creates a visible increase in measured conductance. Catalytic conversion was confirmed by experiments with NO and NO₂ gases. A comparison in response between 5 ppm nitrogen dioxide (red) and nitric oxide (green) for a typical bare CNFET device is shown in Figure 7B. This suggests that a detection of nitrogen dioxide is preferable over pure NO as the last does not show any conductance change.

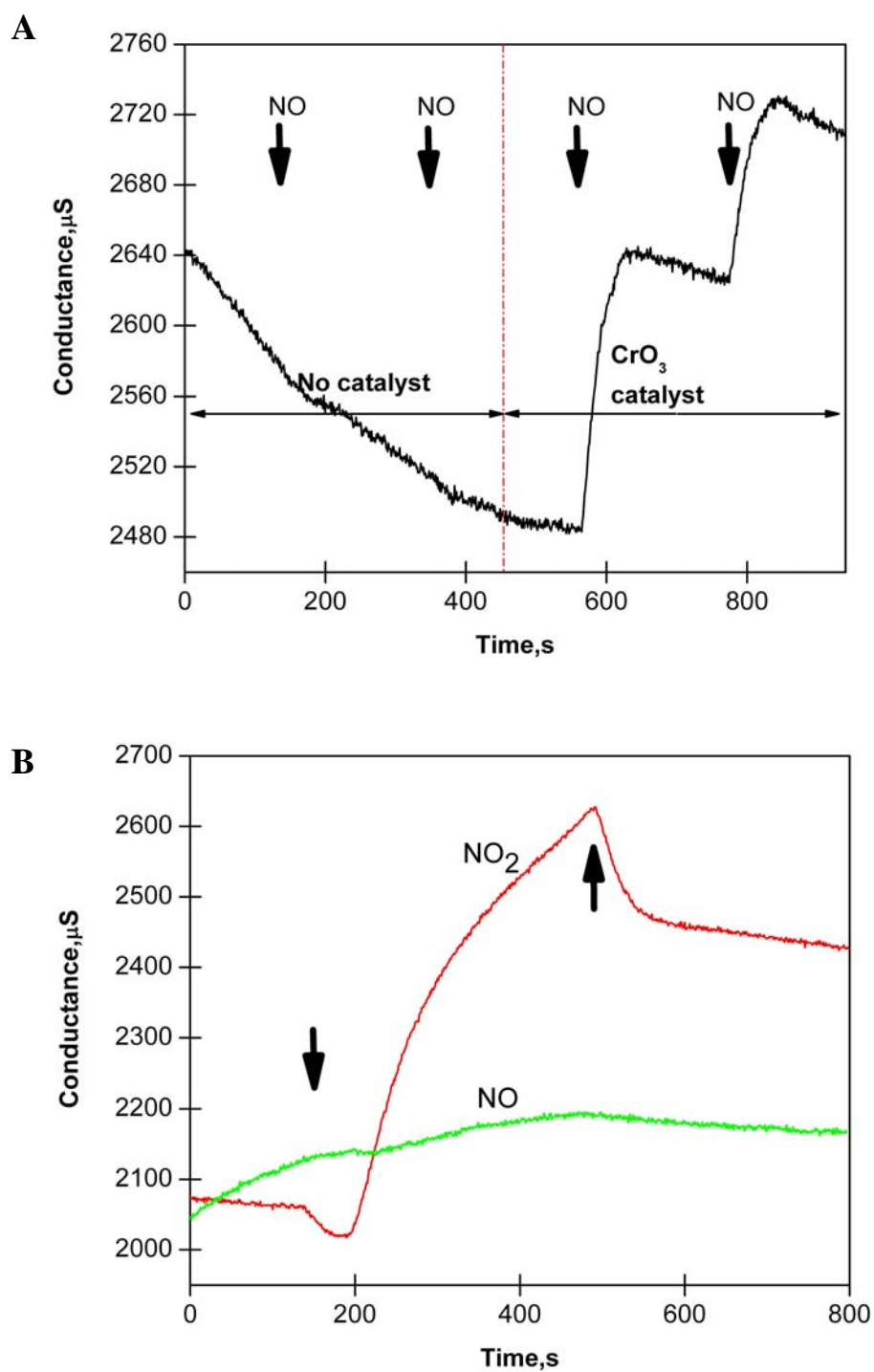


Figure 7. Response of bare NTFET to gases. **(A)** Source-drain conductance versus time for four short pulses of NO gas ($\sim 2\text{ppm}$ in N_2) either bypassing or passing through catalytic converter (CrO_3). **(B)** Comparison of bare NTFET sensor response to 6 min pulses of NO and NO_2 (both $\sim 2\text{ppm}$ in N_2).

Nitric oxide molecule apparently is not capable of transferring charge to a p-type carbon nanotube conducting channel effectively. Thus the number of holes remains unchanged and as a result no conductance change is observed.

Nitrogen dioxide, on the other hand, has strong electron withdrawing properties. By interacting with a carbon nanotube conducting channel, NO₂ molecules are attracting the minority electron carriers. The number of holes in the channel increases and as a result the conductance rise is observed.

In order to improve sensor sensitivity, CNFET devices were functionalized with polymer layers. PEI functionalization of the device surface changes the semiconducting characteristic of the CNFET from p-type to n-type (Figure 8) as was shown previously.^[34]

Bare nanotube devices in oxygen atmosphere typically show p-type behavior. In degassed conditions there is equilibrium between a number of positively charged carbon atoms in the nanotube and a number of free electrons in the conducting channel. Oxygen molecules act as a dopant in this case, by attracting some electrons thus removing them from a channel. This creates a slight excess of holes over electrons and the overall semiconducting characteristic of such carbon nanotubes becomes p-type.

PEI polymer chains contain amino functionalities showing strong electron donating properties. Apparently they introduce large excess of electrons into the nanotube conducting channel to the extent that they become dominant charge carriers. This explains well why an inversion of semiconducting type from **p** to **n** takes place. An alternative explanation of conductance change lies in the fact that carbon nanotubes form a so called Schottky barriers on the interface with a metal electrode.^[35] As a result of a

molecular adsorption on a semiconductor (carbon nanotube)-metal (gold electrode) interface a metal work function changes which in turn modifies the height of a barrier that is proportional to the conductance.

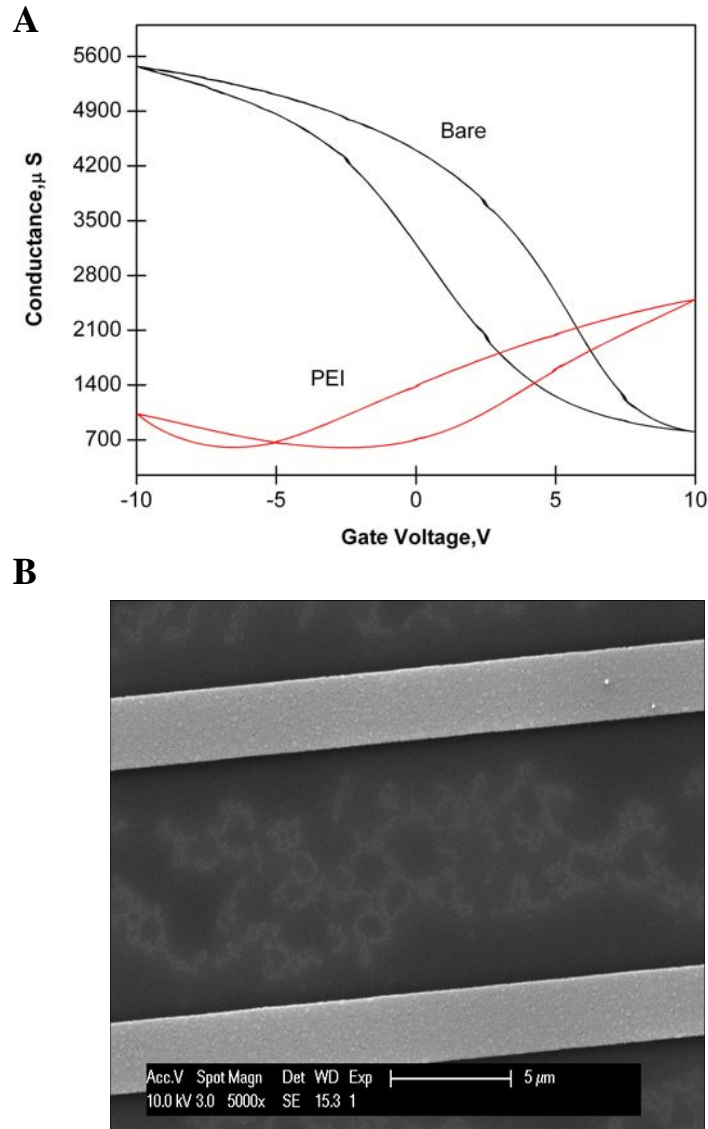


Figure 8. (A) Source-drain conductance versus applied gate voltage for bare and polymer coated NTFET used in this study. (Whereas bare NTFET is p-type, after PEI coating device behaves as n-type transistor). (B) Scanning electron microscopy (SEM) image showing part of two interdigitated electrodes connecting SWNT network after coating with polymer.

3.1 Sensor Dynamic Range

As can be seen, conductance drops when a PEI-functionalized device is exposed

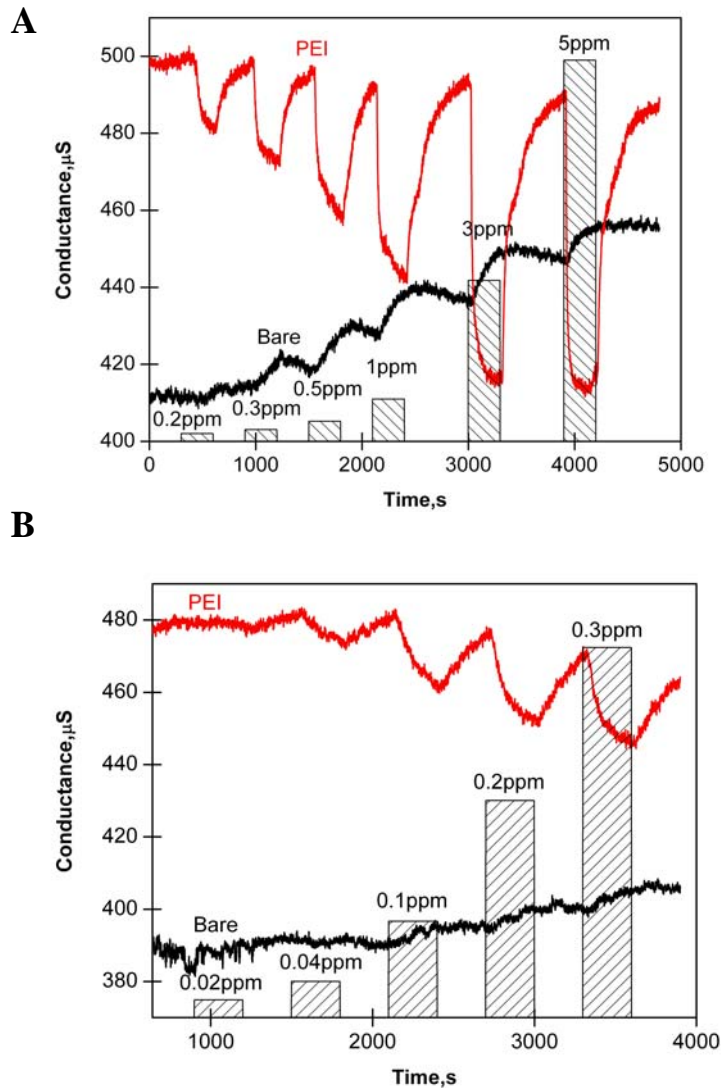


Figure 9. Dynamic range of NO sensor based on bare and polymer coated NTFET devices: Conductance versus time dependence of bare (black trace) and PEI coated (red trace) NTFET devices exposed to six short NO gas pulses of various concentrations. (A) Concentration range between 0.2 PPM and 5 PPM. (B) NO concentrations between 0.02 PPM and 0.3 PPM.

to series of concentrations of NO gas (Figures 9 A, B) that is passed through the catalyst converter (red). Also, in comparison with the bare device (black), the sensor response signal is higher and the recovery characteristics are better. A calibration curve in the concentration range between 20 ppbv and 300 ppbv is given for PEI functionalized and bare devices (Figure 10 A, B).

In the case of PEI modified carbon nanotube FET, the dominant charge carriers are electrons. Nitrogen dioxide molecule may interact with a conductance channel of a nanotube when adsorbed on a nanotube wall (or in the direct vicinity of the wall) by attracting free electron charge carriers. This explains why conductance drops in the presence of NO₂ for PEI coated device.

Up to date, PEI-coated device shows an overall detection limit of around 5 ppbv in inert atmosphere with 15-30 % RH (Figure 11 A). For the bare device, however, the ultimate detection limit lies somewhere between 200 and 300 ppbv. It was also noticed that after two weeks of sporadic exposure to analyte gas the response to the same concentration of gas decreases, which can be explained by some effect of degradation of the PEI polymer.

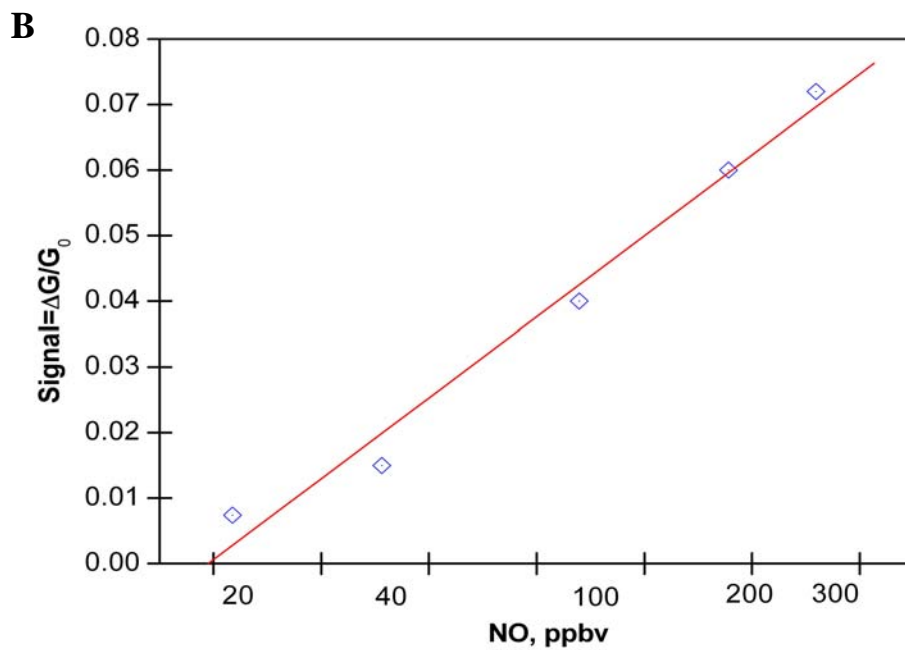
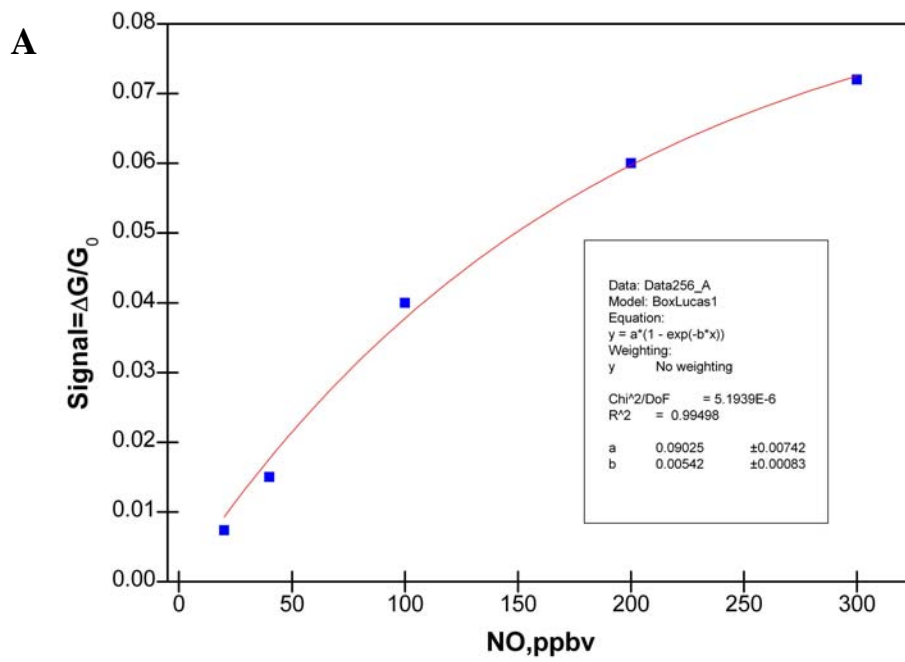


Figure 10. Calibration curve of PEI coated sensor in ppbv range. **(A)** Experimental calibration curve approximated by equation $\text{signal} = 0.09(1 - \exp(-0.054[\text{NO}]))$. **(B)** Same dependence presented on natural logarithm scale

3.2 Cross Sensitivity to Main Breath Components

Cross sensitivity to CO₂ and oxygen was also investigated. The results for carbon dioxide (Figure 11B) show that PEI-coated devices are cross-sensitive to CO₂ in the range 1-6% volume. In the atmosphere of 6% CO₂ detection of low concentrations of NO converted into NO₂ becomes impossible. Thus a scrubber for CO₂ removal is needed. However, bare device does not respond to the same concentrations of CO₂ (data not shown). Oxygen on the other hand (~16 % volume), does not seem to prevent the detection of analyte gas in this concentration range (Figure 11 C).

4 Conclusions

Detection of NO using chemically functionalized carbon nanotubes has been demonstrated in the presented work. It shows a high degree of sensitivity and selectivity towards NO/NO₂ over oxygen. Provided that CO₂ is removed from the analyzed gas mixture by means of trap, the requirements for a human breath nitric oxide sensor could be met.

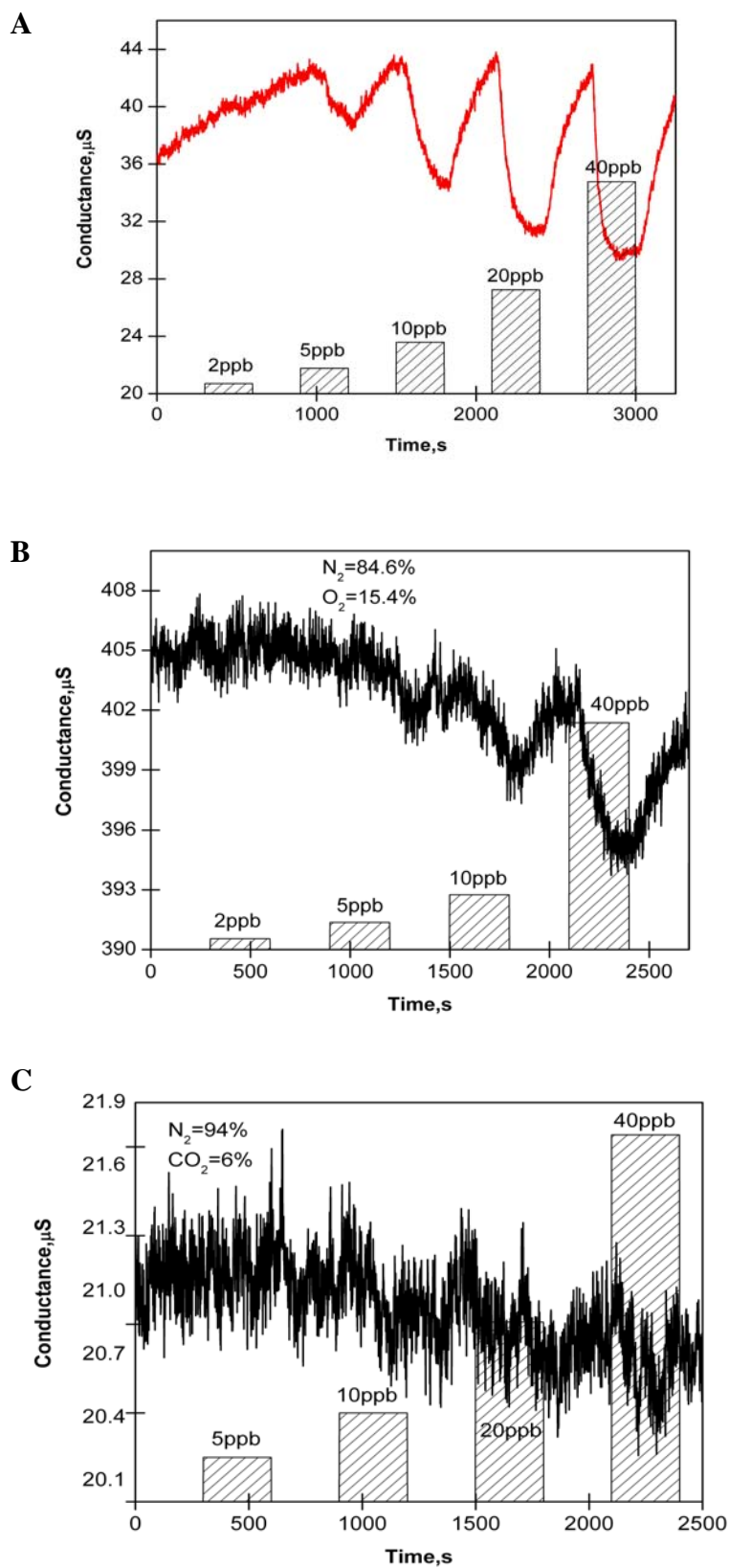


Figure 11. Conductance versus time dependence of PEI coated NTFET device exposed to five short pulses of NO gas at concentration range between 2 PPB and 40 ppb in (A) 100% nitrogen atmosphere, (B) 16% oxygen balanced with nitrogen, (C) 6% carbon dioxide and nitrogen

5 Acknowledgments

We gratefully acknowledge the support provided by Nanomix, Inc. to the group of Alexander Star at the University of Pittsburgh.

PART II

Interactions of Carbon Nanotubes with Metalloporphyrins

(Published in Kauffman, D. R.; Kuzmych, O.; Star, A. "Interactions between Single-Walled Carbon Nanotubes and Tetraphenyl Metalloporphyrins: Correlation between Spectroscopic and FET Measurements", *J. Phys. Chem. C* **2007**, *111*, 3539-3543).

Porphyrins are an extensively studied group of organic molecules which importance as a biological agent and much interest has been generated in exploiting their natural biochemical behavior.^[36,37] Research into this rich field has produced developments such as gas^[38,39,40,41] and electrochemical sensors,^[42,43] and the design of integral components for solar energy conversion.^[44] Compared to porphyrin research the field of carbon nanotube chemistry is still in its infancy,^[45] and much can be learned from coupling the well studied porphyrin to the relatively new nanotube systems. Interest has been gaining in carbon nanotube research due, in part, to the carbon nanotube's potential for such applications as molecular electronics,^[46,47] sensing devices^[48,49] and catalytic platforms,^[50] to name a few. Due to carbon nanotube's environmentally sensitive electronic properties, which can be probed by various spectroscopic^[51,52] and electronic^[44,45,53,54,55] methods, they represent an ideal candidate for nano-scale devices for extremely sensitive applications. Pairing the carbon nanotube with a system having photoactive properties, molecular selectivity, and electron donating characteristics invites the possibility for the development of ultra sensitive and compact devices for a host of energy conversion, analyte sensing, and catalytic capabilities on a truly molecular level. Studies have been conducted on the functionalization of single-walled carbon nanotubes

(SWNT) with porphyrin systems.^[56,57] Recently the interaction between SWNT and porphyrins has led to the creation of supramolecular assemblies^[58] and the study of light induced charge transfer^[59] for applications in solar energy conversion systems. In light of the budding interest in SWNT-porphyrin systems it is important to understand the result of the complexation between the two species in terms of the impact on the electronic structure of the newly formed complex. Combining two techniques such as spectroscopy and NTFET transfer characteristic, i.e. the source-drain conductance dependence on gate voltage, $G-V_G$ response creates a powerful tool for probing SWNT electronic structure, and recently has been used independently to monitor DNA hybridization^[60,61] and conformational changes^[62] on the SWNT surface. In this study we combine UV-Vis-NIR thin-film absorption spectroscopy and NTFET $G-V_G$ measurements to quantitatively address the electronic consequences of porphyrin complex formation on the SWNT electronic structure; specifically the lower energy first and second semiconducting valence bands.

Purified SWNT (Carbon Solutions) were dispersed in DMF and sonicated for approximately 30 minutes until the solution became uniform in color, indicating good nanotube dispersion. 5,10,15,20-Tetraphenyl-21H,23H-porphine manganese(III) chloride (MnTPP), zinc(II) (ZnTPP), copper(II) (CuTPP), and cobalt(II) (CoTPP) tetraphenyl porphyrins (Sigma-Aldrich) were dissolved in DMF and introduced in excess to the SWNT solution. An additional 5 minute sonication was conducted to ensure even distribution of SWNT and M-TPP and facilitate complex formation. After stirring overnight the solution was filtered and rinsed with copious amounts of DMF, water and acetone to remove any free M-TPP, and dried in vacuum. The dried SWNT/M-TPP

filtrate was redispersed in DMF by brief sonication and used for solution UV-Vis absorption spectroscopy or sprayed onto a heated quartz substrate with a commercial air brush (Iwata) to create SWNT/M-TPP thinfilms, which afterwards were dried under vacuum and used for spectroscopic measurements on a Lamda 900 UV-Vis-NIR spectrophotometer (Perkin Elmer). NTFET devices were constructed as described elsewhere,^[58] but briefly, SWNTs were grown via CVD process onto Si wafers and interdigitated gold electrodes were photolithographically patterned onto the SWNT network creating multiple devices on the Si chips. For experiments, chips were wire-bonded and packaged in a 40-pin CERamic Dual-Inline Package (CERDIP) and tested using a custom NTFET electronic test fixture.^[58] NTFET devices were complexed with M-TPP by dropcasting a small volume of metalloporphyrin solution (1 μ L, 10^{-4} M in THF or DMF) onto the NT network and source-drain conductance versus gate voltage ($G-V_G$) transistor characteristics were recorded.

Figure 12A shows the UV-Vis-NIR spectra taken using thinfilms on a thin (\sim 1 mm) quartz substrate of pure SWNT and the SWNT/MnTPP complex, clearly showing the first two semiconducting and metallic electronic transitions, referred to as the S_1 , S_2 and M_1 bands, respectively. The origin and significance of SWNT transition bands is well described in the literature.^[63,64,65] The thin film absorption spectra reveal two interesting characteristics about the interaction between SWNT and the MnTPP. First, a substantial redshift in the S_1 absorption band can be seen. Pure SWNT have a S_1 absorption band centered around 1845 nm, but upon complexation with MnTPP the S_1 band is shifted to 1895 nm, a 50 nm (16 meV) redshift. In addition a redshift of 12 meV was seen in the S_2 absorption band. Secondly, the M_1 and S_3 (not shown) were not shifted

by the addition of MnTPP. Figure 12B shows the results of SWNT source-drain conductance versus gate voltage ($G-V_G$) measurements of an unfunctionalized (blue) and MnTPP functionalized (red) NTFET. Two important observations can be made from this data, the first being an obvious negative shift in the gate voltage of approximately 2.5 V. Secondly, no change in minimum conductance was seen beyond a positive gate voltage of 5.0 volts. Each NTFET chip has several devices with different separations between interdigitated electrodes (pitch sizes) and different device areas. It was found that shifts in gate voltage were consistent for all device geometries functionalized with the same M-TPP. Additionally, similar $G-V_G$ results were obtained with NTFET chips functionalized with M-TTP solutions made in DMF and THF. The observed phenomenon is explained by an ability of porphyrines to donate electrons to partially filled S_1 band of carbon nanotubes. As M-TTP donates electronic density into the SWNT S_1 , the band gap will decrease (Figure 12), resulting in the observed S_1 red-shift. On the other hand, the electron donation from M-TTP would result in a decrease of the carrier concentration, and the negative gate voltage shifts in M-TTP-functionalized NTFETs $G-V_G$ transfer characteristics are in line with previous findings.^[57]

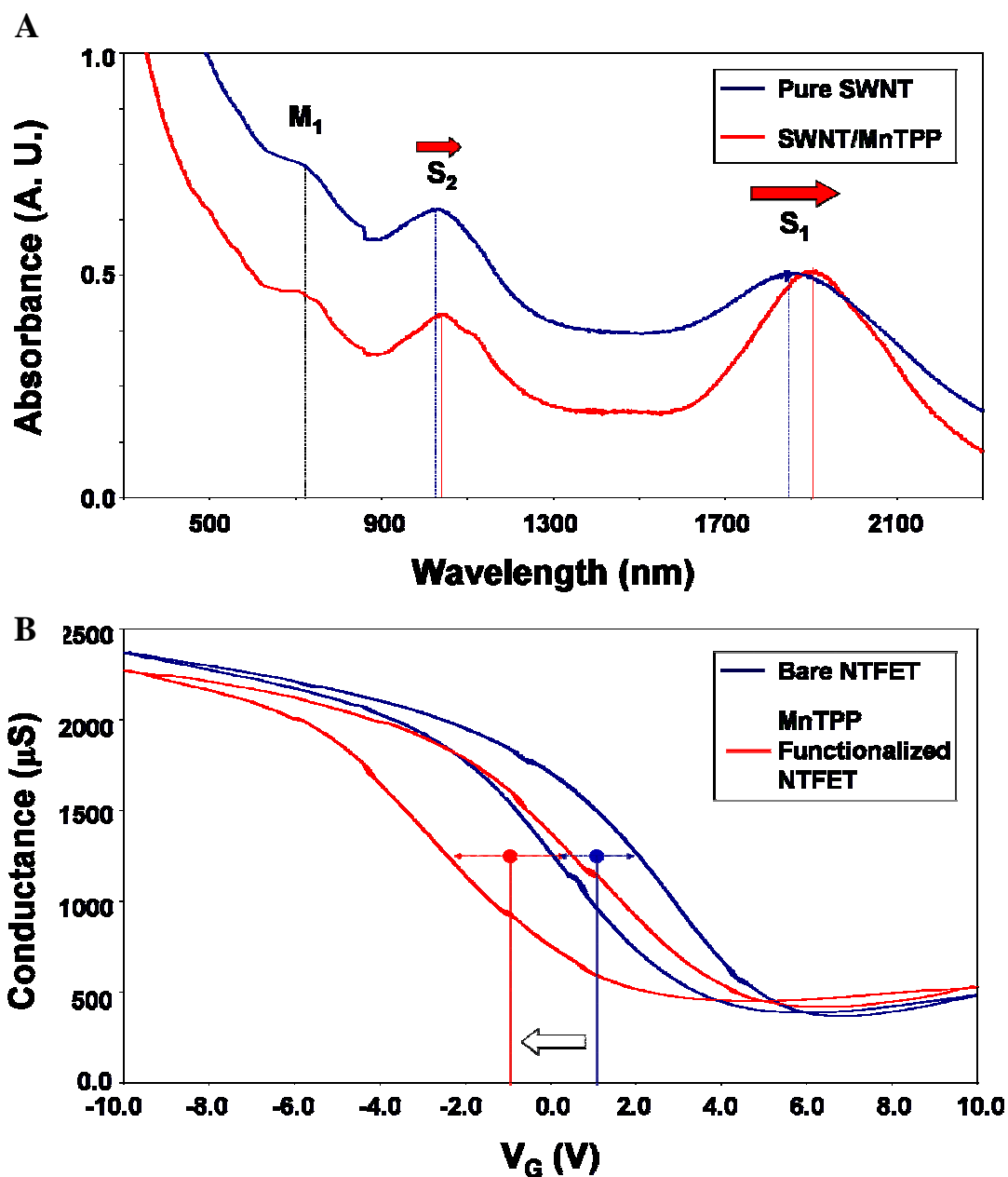


Figure 12: (A) Thinfilm UV-Vis-NIR absorption spectra of pure SWNT (blue) and SWNT-MnTPP (red) showing redshifts in the S_1 and S_2 nanotube absorption bands. (B) Conductance versus gate voltage (V_G) characteristics of bare (blue) and MnTPP functionalized (red) NTFET devices showing a negative shift in gate voltage (arrow) and no decrease in the minimum conductance region positive of 5.0 volts.

PART III

ADSORPTION AND GEOMETRY OF THE CHEMISORBED BENZOATE SPECIES ON Cu (110)

(Published in Lee, J.; Kuzmych, O.; Yates J. T. Jr. “Adsorption and Geometry of the chemisorbed Benzoate Species on Cu (110)”, Surf. Sci. **2005**, 582, 117–124).

INTRODUCTION

The structure of adsorbed organic species is fundamentally important to many areas, including molecular electronics,^[66] the formation of self assembled monolayers^[67] and in organic chemistry on surfaces.^[68] These adsorbates form structures at low coverage which represent the fundamental bonding issues at work in chemisorption. As coverage increases, intermolecular interactions cause modification of the structure of the adsorbate, and it is often observed that twisting and tilting of rigid organic ring structures takes place as these interactions build up.^[69,70] Carboxylic acids are known to deprotonate when chemisorbed on metal surfaces.^[71,72,73,74] Thus acetic acid on Cu (110) produces the acetate species which is known to be bound in a normal orientation to two close-packed Cu atoms on the surface with the plane of the carboxylate moiety being oriented parallel to the <110> azimuth.^[75,76] Studies of the adsorption of benzoic acid indicate that similar bonding of benzoate occurs on Cu(110) and STM studies show that a series of coverage-dependent ordered structures form as the coverage

increases.^[75,77,78,79,80,81,82] It appears that at 183 K and sub monolayer coverage, a mixture of lying-down and normally-oriented benzoate species coexist.^[79] A study of benzoic acid chemisorbed on Ni(110) indicates that the ring is rotated $\pm 30^\circ$ relative to the $\langle 110 \rangle$ azimuth, and is tilted $\sim 30^\circ$ with respect to the surface normal at saturation coverage. Benzoate is chemisorbed in different structures at lower coverages on Ni (110).^[83] On the TiO₂ (110) surface, the benzoate species is bonded through the carboxyl group with the five-fold coordinate Ti⁴⁺ cations, and forms an ordered pseudo-(2x1) overlayer at a saturation coverage of 0.5 ML.^[84] A high resolution electron energy loss spectroscopy (HREELS) study of the adsorption of benzoic acid adsorbed on Na-Si(100)-(2x1) shows that benzoate is bonded in bidentate coordination at room temperature and in monodentate coordination on the clean Si(10 0) surface.^[85] In this paper, we have studied the adsorption of benzoic acid and the surface conformation of the benzoate species formed from benzoic acid on Cu(110). This investigation is part of our effort to define the behavior of small chemisorbed molecules which can be used as models for more complex molecules that may be useful as molecular electronic devices.

EXPERIMENTAL

The experiments described in this work have been carried out in an ultrahigh vacuum system with a base pressure below 1×10^{-10} mbar, as described elsewhere.^[76] The Cu(110) single crystal was 10 mm in diameter and 2 mm thick, and could be cooled down

to 81 K and electrically heated to 900 K. It was cleaned by Ar⁺ bombardment, followed by annealing in vacuum at 800 K. The final Auger spectrum obtained with a PHI model 10-155 CMA indicates that all impurities such as S and O are below the limits of detection. A sharp (1x1) low energy electron diffraction (LEED) pattern, characteristic of Cu (110), is routinely observed. The electron stimulated desorption ion angular distribution (ESDIAD) method is the principal measurement technique employed here.

The ESDIAD/LEED optics are described in a previous paper, and the TOF-ESDIAD method, specifically separating H⁺ ions from others, is employed in these measurements.^[86] All ESDIAD patterns are compressed by the use of a +30 V crystal bias, except for the emission angle versus crystal bias measurements. The incident electron beam energy is fixed at 180 eV. A heated doser system was employed for exposing the crystal to gases with a low vapor pressure.^[87] The pressure in the UHV system rises by about 2×10^{-10} mbar during dosing. All exposures were carried out at a crystal temperature of 81 K. Because the benzoic acid dissociates to form benzoate species in the first monolayer, we could not use temperature programmed desorption to observe the first stage of adsorption of benzoic acid up to the saturation coverage of benzoate. Therefore, calibration of the relative coverages was carried out using the C(KLL) Auger intensity, and a linear plot of coverage versus exposure time was obtained below the saturated monolayer coverage as shown in Fig. 13. At exposures longer than 130 s, the desorption of undissociated benzoic acid occurs as shown in the inset to Fig. 13. Only a small effect on the C(KLL) intensity was induced by the electron beam of the Auger spectrometer as shown in Fig. 14. A UTI 100C quadrupole mass spectrometer (QMS) was used for temperature programmed desorption (TPD) studies for benzoic acid.

It was shielded from the crystal by a grid biased at -75 V to eliminate spurious electron bombardment from the thermionic emitter in the mass spectrometer, which was separately shown to influence the TPD measurements slightly. The electron ionization energy employed in the mass spectrometer

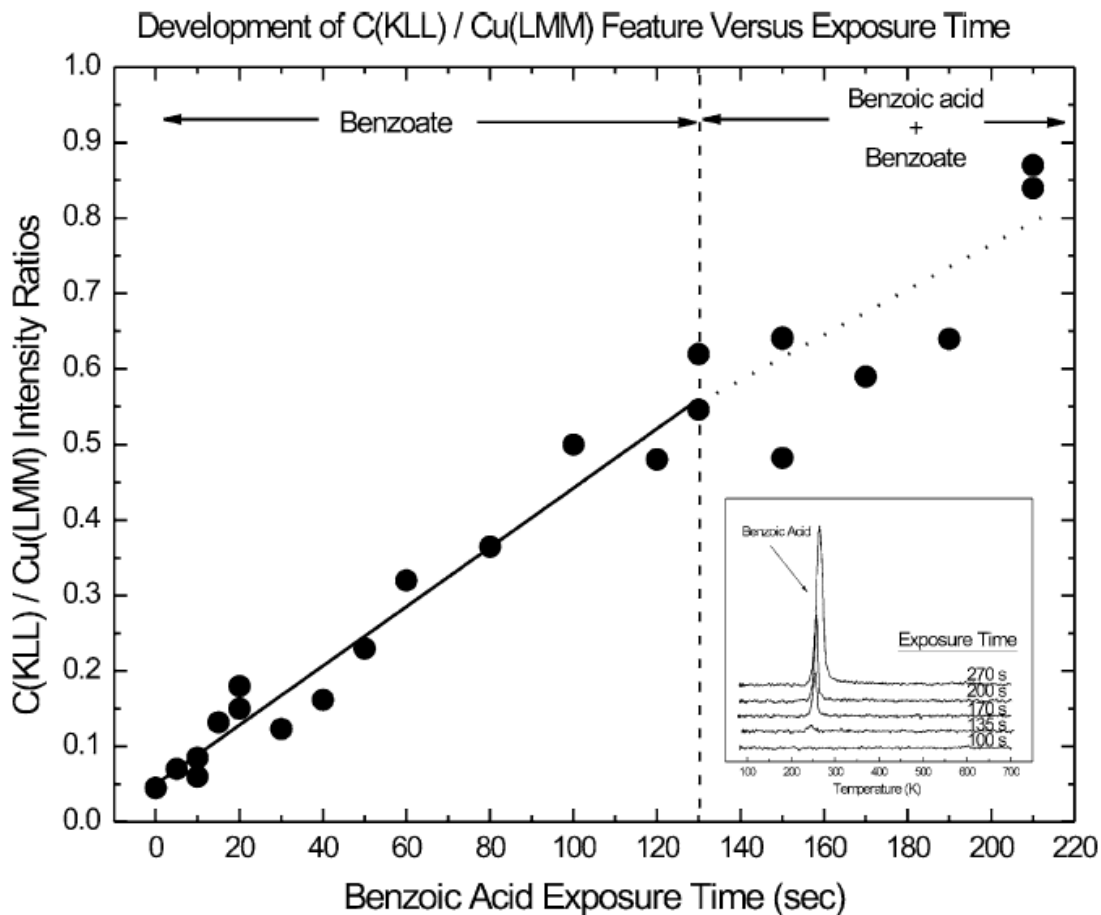


Figure 13. Development of the C(KLL) Auger feature versus exposure to benzoic acid from the heated doser source. The end of the first monolayer of dissociative adsorption is indicated as condensed benzoic acid begins to be observed by thermal desorption (see insert).

Effect of Electron Beam on C(KLL) Auger Signal for Benzoic Acid

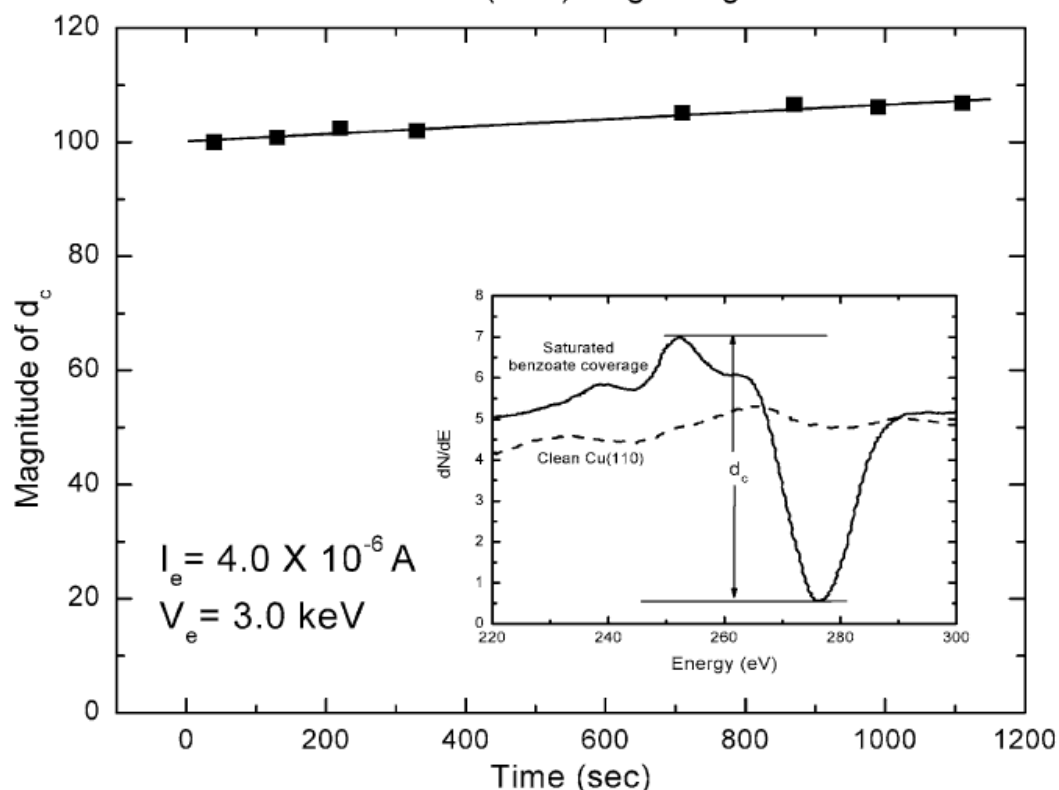


Figure 14. Study of the effect of electron bombardment on the C(KLL) Auger intensity, showing that AES may be used to measure the coverage. Inset shows the Auger spectra for clean Cu(110) (dashed line) and for a saturated coverage of benzoate (solid line). The initial magnitude of d_c is assigned as 100. The slight increase in d_c is probably due to slow adsorption of benzoic acid from the background gas.

was 70 eV. The mass spectrometer fragment at 105 amu was used to monitor the thermal desorption of benzoic acid which represents the parent peak at 122 amu minus 17 amu (OH). The benzoic acid as supplied was 99.5% pure (Aldrich). We found that water is a major impurity when the benzoic acid is heated to 50 °C to achieve the desired vapor pressure in the heated doser system, and further purification of the solid acid in a separate gas handling line was carried out with a turbomolecular pump and with molecular sieve material held in a trap between the sample bulb and the turbomolecular pump.

RESULTS AND DISCUSSION

Fig. 15 shows the TPD spectra of benzoic acid as a function of increasing exposure where just one benzoic acid desorption process can be observed, beginning near 250 K. This desorption feature exhibits typical multilayer behavior as coverage increases, i.e., the leading edges coincide for different initial coverages. This is due to the formation of the multilayer of intact benzoic acid and free-sublimation from the multilayer with zero-order desorption kinetics. In the insert to Fig. 15, a leading-edge analysis of the multilayer benzoic acid desorption yields an activation energy of desorption of 91.5 ± 0.9 kJ/mol, which corresponds within experimental error to the sublimation enthalpy of solid benzoic acid (91.4 kJ/mol).^[88] We shall not be further concerned with the multilayer properties of condensed benzoic acid. It is well known that various carboxylic acids on the Cu(11 0) surface form carboxylate species after adsorption at room temperature or after annealing the surface to higher temperatures.^[72-75] This process occurs via O–H bond scission of the carboxylic acid^[76] and it is known from photoelectron diffraction measurements that the resultant carboxylate species bonds via its O atoms to two close-packed Cu atoms.^[77] According to the studies mentioned, one can expect that there should be benzoate formation from the first monolayer of adsorbed benzoic acid upon heating. The lack of a benzoate thermal desorption peak

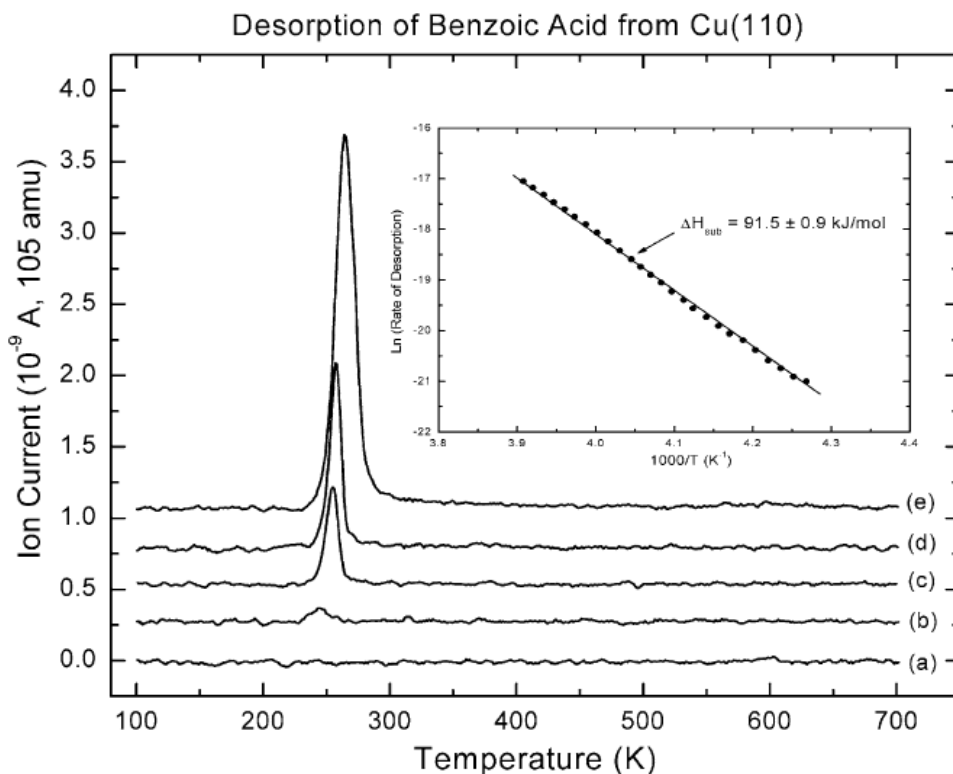


Figure 15. Thermal desorption of benzoic acid from Cu(110). Coverages: (a) 2.2×10^{14} molecules/cm²; (b) 2.8×10^{14} molecules/cm²; (c) 3.5×10^{14} molecules/cm²; (d) 4.3×10^{14} molecules/cm²; (e) 5.6×10^{14} molecules/cm². These coverages were estimated from separate AES measurements of the build up of the C(KLL) Auger intensity shown in Fig. 13 combined with information from LEED measurements.^[81] The insert shows a plot of the kinetics of leading edge desorption of the benzoic acid from which the enthalpy of sublimation of the multilayer can be derived.

is due to the fact that chemisorbed benzoate decomposes into other products and these studies will be presented in detail elsewhere. It is known for some chemisorbed aliphatic carboxylate species that there is a decomposition reaction at high temperature.^[89,90,91] The desorption of benzoate species itself is highly improbable because the activation energy to break the two Cu–O bonds is very high.^[92] Both LEED and STM measurements suggest that the adsorption of benzoic acid results in a saturated benzoate layer with a (8x2) periodicity which corresponds to 0.25 ML.^[81] On this basis, for a saturated chemisorbed layer of benzoate, the coverage is 2.7×10^{14} molecules/cm², i.e.,

0.25 ML, based on the number of surface Cu atoms (1.1×10^{15} atoms/cm²) on the clean surface. Fig. 16 shows a comparison of the thermal desorption behavior of benzoic acid with the H⁺-ESDIAD patterns being obtained after heating a multilayer/monolayer deposit to various temperatures. In Fig. 16a, two desorption traces are superimposed. The 44 amu trace due to CO₂ desorption occurs from the first monolayer of benzoate which decomposes above 500 K. The 105 amu trace is due to undissociated benzoic acid in the second and higher layers as illustrated in Fig. 15. In Fig. 16b, the H⁺-ESDIAD patterns for benzoic acid adsorption to multilayer coverage is shown beginning at 81 K and continuing upward in temperature to 530 K. The surface was cooled to 81 K before making the ESDIAD measurements in each case. Below about 300 K, the H⁺-ESDIAD patterns are intense and consist only of a broad normal H⁺ beam. This type of pattern is often seen for organic molecules at high coverage and is thought to be due to a random distribution of H⁺ beam emission directions caused by random orientation of the adsorbate molecules.

Above temperatures of about 300 K, a three beam H⁺-ESDIAD pattern begins to be observed after the multilayer of benzoic acid has been removed by heating. This pattern, due to chemisorbed benzoate, becomes most sharply defined after heating to 510 K, probably as a result of adsorbate ordering. Above about 530 K, as decomposition of the benzoate occurs, the distinctive three-beam H⁺ pattern disappears. The three-beam pattern exhibits a central H⁺ beam which is most intense.

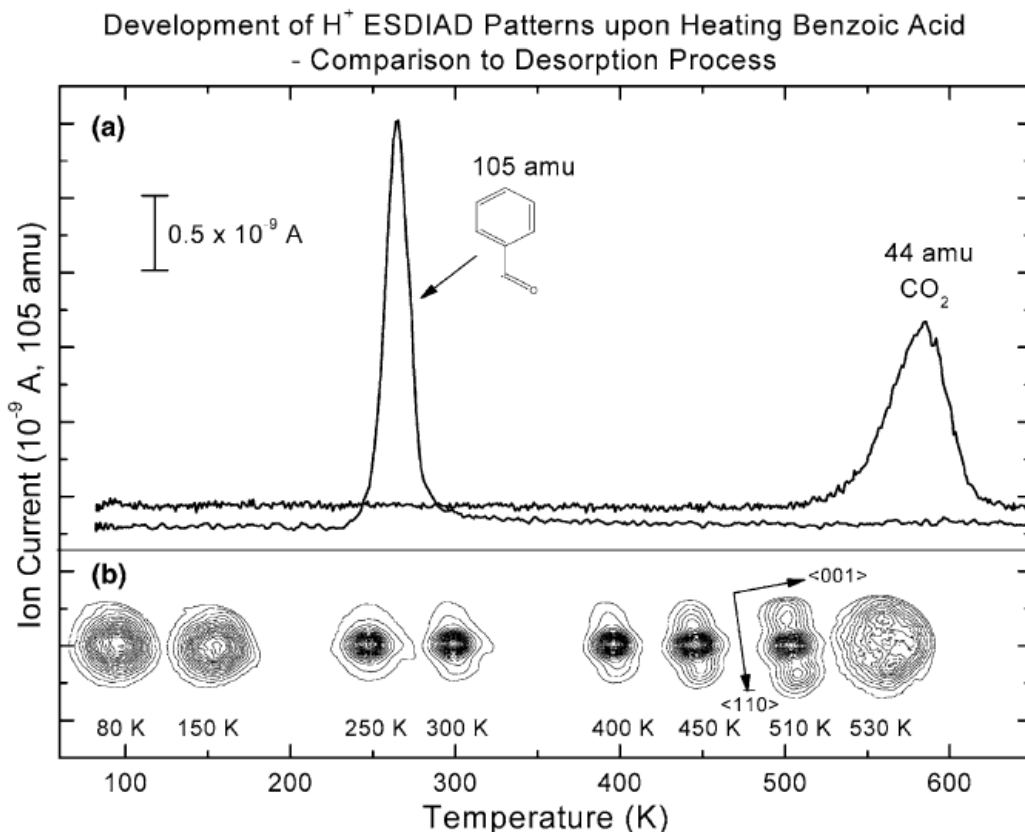


Figure 16. Development of H⁺- ESDIAD patterns upon heating revealing the normally-oriented benzoate species above 300 K at 0.25 ML coverage. Initial coverage = 5.6×10^{14} molecules/cm².

The two “shoulder” beams are accurately aligned along the <110> crystal azimuth, indicating that the phenyl ring is aligned parallel to this direction at low coverages. The central H⁺ beam exactly corresponds to the surface normal direction which indicates that the benzoate species adsorbs perpendicular to the surface. No other heavier positive ion fragments of benzoate are observed, probably due to ion neutralization effects at the surface. Fig. 17 shows a three-dimensional view of the three-beam H⁺-ESDIAD pattern as well as a section through the center of the pattern in a plane parallel to the <110> azimuth. H⁺ desorption is observed from the 3-, 4-, and 5-positions on the phenyl ring. The three H⁺ beams have been deconvolved into three Gaussian peaks as shown. The

relative integrated intensity of the H^+ beams is $I^+(3, 5)/I^+(4) \sim 0.4$. The polar angle of emission of the inclined H^+ beams relative to the normal can be estimated from the measured ion emission angle versus the bias voltage of crystal. This analysis is shown in Fig. 18, where the measured beam angles versus crystal bias voltage are plotted, and compared to the known ion-optical properties of the analyzer; the plot shows an extrapolation to zero bias, yielding the true ion emission angle of $53 \pm 1^\circ$ corrected for the ion optics of the ESDIAD analyzer system.^[93] The estimated H^+ kinetic energy which best fits the data is $E_H^+ = 1.1$ eV; the TOF analysis of the H^+ ion energy yields $E_H^+ = 1.2$ eV, in good agreement with the estimate from the ion-optical fit shown in Fig. 15. In order to determine the C–H bond angles for the inclined C–H bonds in the 3- and 5-positions on the benzoate species, the measured H^+ ion emission angles must be corrected for final state effects involving charge neutralization and image potential effects, following the method of Miskovic et al.^[94,95] This correction amounts to $+11^\circ$. Thus the bond angle with respect to the normal for the C–H bonds at the 3- and 5-positions is 64° . This compares fairly well to the known angle between C–H bonds of 60° for the phenyl group. Fig. 19 shows the structure of a chemisorbed benzoate species on Cu(110) as deduced from these studies at 0.25 ML coverage.

The observation of the central H^+ beam oriented normally to the Cu(110) surface indicates that the axis of the carboxylate species is oriented normally to the surface at saturation coverage used in this experiment. This result is consistent with knowledge from other experiments. For example, the acetate species has been found to be normally oriented on Cu(110) by several methods,^[92] including ESDIAD.^[76] The orientation of

H^+ beams from carbon atoms at the 3- and 5-positions on the phenyl ring further substantiates the normal orientation of the benzoate species. In addition, since the H^+ ions originating from the 3-, 4- and 5-C–H bonds are oriented in a plane parallel the $\langle 110 \rangle$ azimuth, this observation clearly shows that the plane of the molecule is parallel to the $\langle 110 \rangle$ azimuth on the surface and that two close-packed Cu atoms in the surface must bond to the O atoms of the carboxylate group, giving this molecular orientation. The separation between the two close packed Cu atoms is 2.55 \AA , whereas the O–O separation in the unbonded carboxylate group in benzoate is 2.22 \AA .^[81] The measured angle of 64° between corrected H^+ emission direc-

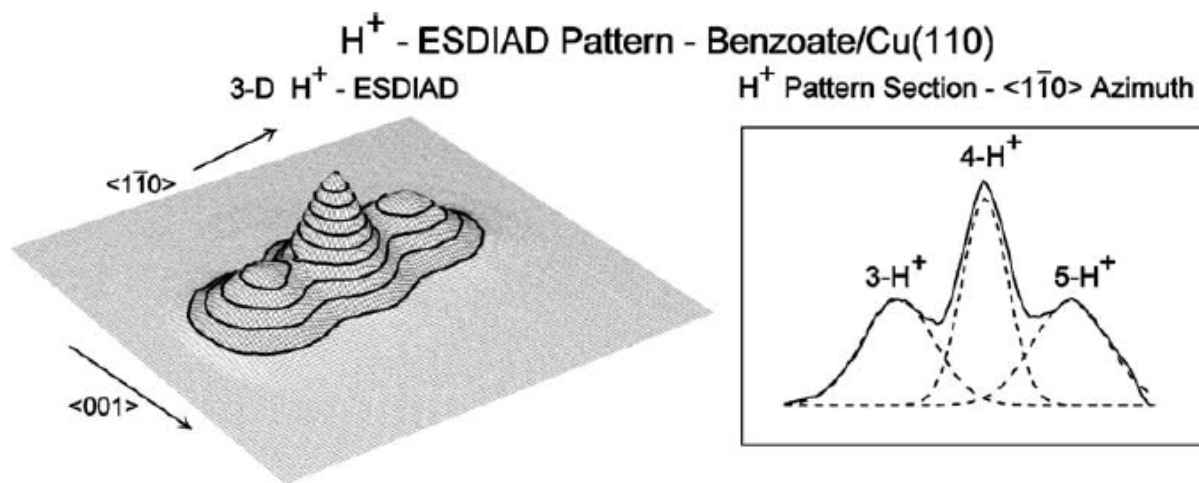


Figure 17. H^+ ESDIAD patterns for benzoate on Cu(110). The image was taken after adsorption of a multilayer of benzoic acid and annealing the sample to 480 K to desorb the benzoic acid and to order the benzoate layer.

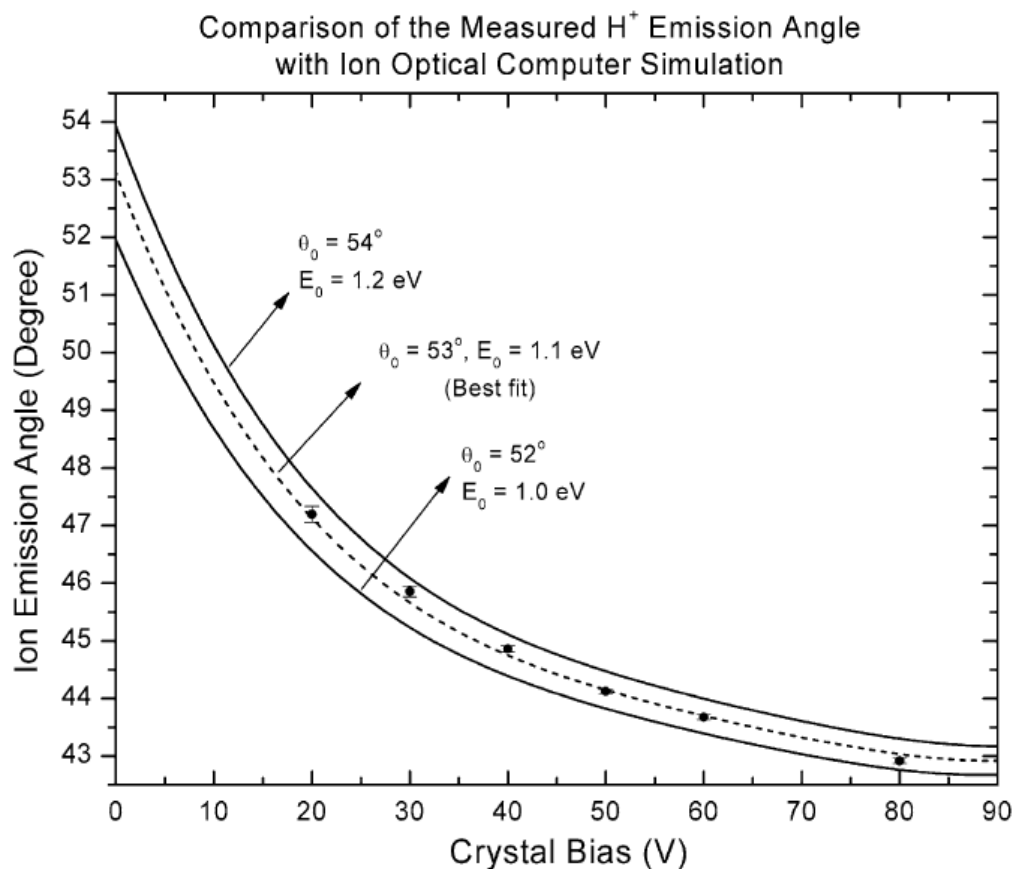


Figure 18. Measured H⁺ polar emission angle for the 3- and 5-positions of the chemisorbed benzoate species on Cu(110). The lines are computer simulations of an ion-optical model for the ion emission angle as a function of crystal bias voltage. The error bars represent the errors in determining the angle between the H⁺ ion beams from the 3-, 5- and 4-H⁺ position, using the Gaussian fitting function.

tions in the 3, 5 and 4 positions differs by 4° from the known C–H bond directions in the phenyl group. We believe this difference is due to our inability to exactly correct for the final state effect on the H⁺ ion beam directions using the method in Refs.^[95, 96]

SUMMARY

The following results concerning the adsorption of benzoic acid and its decomposition to benzoate on Cu(110) has been obtained:

1. Benzoic acid adsorbs into a multilayer on Cu(110). Desorption via zero order kinetics occurs with an activation energy equal to the sublimation enthalpy of bulk benzoic acid.
2. The first monolayer of benzoic acid dissociates below 300 K to benzoate species.^[48]
3. H⁺-ESDIAD studies of H⁺ ejection from the 3-, 4-, and 5-C-H bond position in chemisorbed benzoate yield 3 sharp beams aligned along the <110> azimuth. The normal 4-H⁺ beam

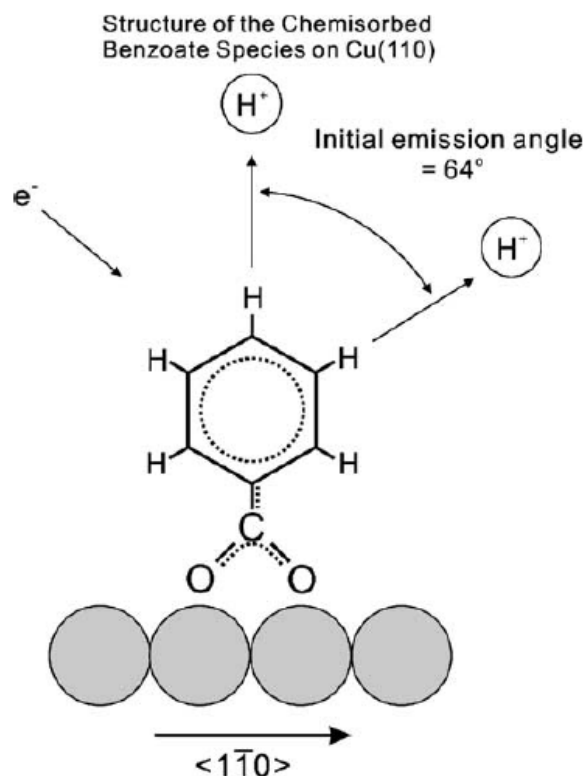


Figure 19. Structure of the chemisorbed benzoate species on Cu(110). The initial H⁺ emission angle is also indicated which is corrected for the neutralization and the image charge final state effects on H⁺ ions. Coverage = 0.25 ML.

indicates that the principal axis of the benzoate species is oriented normally to the Cu(110) surface at 0.25 ML coverage. This implies that the benzoate species bonds to 2 close packed Cu atom in the Cu(110) surface.

4. The H⁺ ion emission angles from the 3- and 5- C–H positions are tilted 64° from the surface normal. An expected tilt angle of 60° suggests that corrections for final state effects on the escaping H⁺ ions may be slightly in error.

5. ESD of H⁺ from the phenyl group of benzoate occurs yielding an H⁺ kinetic energy of 1.1–1.2 eV.

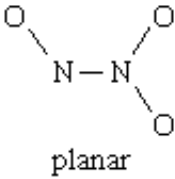
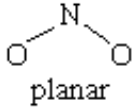
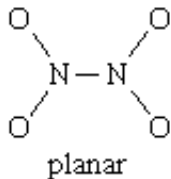
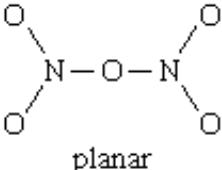
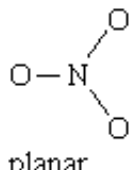
ACKNOWLEDGMENTS

We gratefully acknowledge support by the W. M. Keck Foundation to the W. M. Keck Center for Molecular Electronics, located in the Surface Science Center, and by a NEDO grant from Japan.

Appendix A

Nitrogen Oxides (NO_x) Chemistry Overview

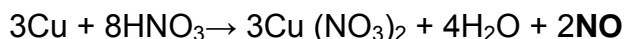
Nitrogen reacts with oxygen to form several nitrogen oxides (NO_x), in which nitrogen exhibits oxidation states from +1 to +5. The following table lists all NO_x compounds in a convenient single-page format.

The Oxides of Nitrogen			
name	formula	structure	description
Dinitrogen monoxide (nitrous oxide)	N_2O	$N-N-O$ linear	colourless gas (bp $-88.5^\circ C$)
(Mono)nitrogen monoxide (nitric oxide)	NO	$N-O$	colourless paramagnetic gas (bp $-151.8^\circ C$); liquid and solid are also colourless when pure
Dinitrogen trioxide	N_2O_3	 planar	blue solid (mp $-100.7^\circ C$); dissociates reversibly in gas phase to NO and NO_2
Nitrogen dioxide	NO_2	 planar	brown paramagnetic gas; dimerizes reversibly to N_2O_4
Dinitrogen tetroxide	N_2O_4	 planar	colourless liquid (mp $-11.2^\circ C$); dissociates reversibly in gas phase to NO_2
Dinitrogen pentoxide	N_2O_5 $[NO_2]^+[NO_3]^-$	 planar	colourless ionic solid; sublimes at $32.4^\circ C$ to unstable molecular gas ($N-O-N$ angle $\sim 180^\circ$)
Nitrogen trioxide	NO_3	 planar	unstable paramagnetic radical

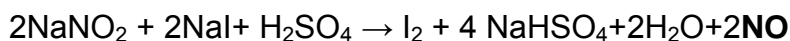
Source: Reprinted from N.N. Greenwood and A. Earnshaw, *Chemistry of the Elements*, copyright © 1984, p. 509, with kind permission from Butterworth-Heinemann Ltd.

Nitrous oxide (N₂O) is a colorless gas with a mild, pleasing odor and sweet taste. It is broadly used as anesthetic gas, especially in dentistry, and is called laughing gas because of its intoxicating effect. This gas has very small potential for oxidation of organic substances and strong reducing agents.

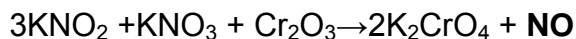
Nitric oxide (NO) naturally forms during lightning storms when oxygen directly combines with nitrogen. In industry it is produced by the reaction of dilute nitric acid with copper or catalytic oxidation of ammonia:



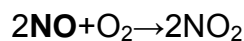
Gaseous nitric oxide is the most thermally stable oxide of nitrogen and is also the simplest known thermally stable paramagnetic molecule – i.e., a molecule with an unpaired electron. For this reason, NO can be detected using Electron Spin Resonance (ESR) spectroscopy method. It is one of the environmental pollutants generated by internal-combustion engines, resulting from the reaction of nitrogen-containing compounds in fuel (mainly indoles, carbazoles, pyridines, and quinolines) and oxygen during the combustion process. Pure NO can be obtained by aqueous



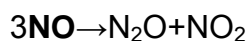
or dry reactions.



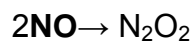
Nitric oxide reacts instantly with oxygen:



In general, it can be reduced to nitrous oxide or oxidized by strong agents such as F_2 , Cl_2 and Br_2 . Nitric oxide is thermodynamically unstable at 25°C and 1atm and under pressure readily decomposes in the range 30 to 50°C :



Because of one unpaired electron in an anti-bonding orbital, NO readily forms nitrosonium ion (NO^+), which is stable and has a rich chemistry. At room temperature nitric oxide is a colorless gas consisting of diatomic molecules. However, because of the unpaired electron, two molecules can combine to form a dimer by coupling their unpaired electrons.

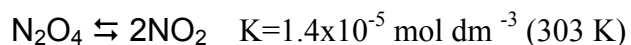


Thus, liquid nitric oxide is partially dimerized, and the solid consists solely of dimers. The solubility of NO in water at 0°C is around 7.3 %. When a mixture of equal parts of nitric oxide and nitrogen dioxide, NO_2 , is cooled to -21°C (-6°F), the gases form dinitrogen trioxide, a blue liquid consisting of N_2O_3 molecules. This molecule exists only in the liquid and solid states. When heated, it forms a mixture of NO and NO_2 . Nitrogen dioxide is prepared commercially by oxidizing NO with air, but it can be prepared in the laboratory by heating the nitrate of a heavy metal, as in the following equation:

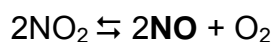


This method, however, does not give a high purity product.

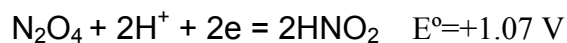
Nitrogen dioxide (NO₂) and dinitrogen tetroxide (N₂O₄) exist in a strongly temperature-dependent equilibrium:



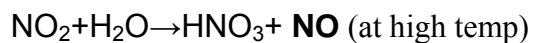
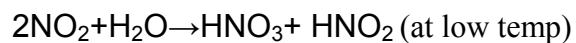
The dimer is colorless where as the monomer is deep brown in color. The thermal decomposition of NO₂ starts at 150 °C and is completed at 600°C.



The oxides are fairly strong oxidizing agents in aqueous solution and comparable in strength to bromine:



The gases are highly toxic and attack metals rapidly. They react with water:

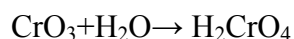


Overall, in their chemical activity, the nitrogen oxides undergo extensive oxidation-reduction reactions.

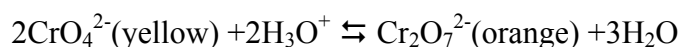
Appendix B

Chromium Trioxide Catalyst Chemistry Overview

Chromium trioxide (CrO_3) is a substance where element chromium shows its highest oxidation state (+6). The substance dissolves readily in water forming chromic acid H_2CrO_4 ,



which can not be isolated as a pure substance and exists only in ionic form in water solution. A pH-dependant equilibrium between chromates and dichromates is established:



On the surface of solid chromium trioxide in the presence of water vapor, a liquid layer containing chromates is formed which gives it an orange/red color (Figure 20B). It is

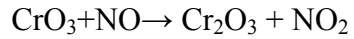
A

B

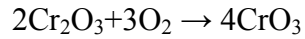


Figure 20. Color of chromium oxide catalyst depending on dominant state of oxidation. **A: +3, B: +6**

able to oxidize many organic and inorganic substances including nitric oxide (NO):



The chromium trioxide gets reduced to Chromium (III) oxide which has a green/brown color (Figure 20A). Nitric oxide gets reduced to nitrogen dioxide (NO₂). In the presence of air CrO₃ acts as a true catalyst as the Cr₂O₃ gets oxidized back to +6 state:



It was experimentally established, however, that for small doses of nitric oxide (ppb) the catalyst remains active for relatively long time even in inert atmosphere.

References

- (1) Gustafsson, L. E.; Leone, A. M.; Persson, M. G.; Wiklund, N. P.; Moncada, S. *Biochem. Biophys. Res. Commun.* **1991**, *181*, 852–857.
- (2) Bernareggi M.; Cremona G. *Pulmonary Pharmacology & Therapeutics* **1999**, *12*, 331-352.
- (3) Gill, M.; Walker, S.; Khan, A.; Green, S. M.; Kim, L.; Gray, S.; Krauss, B. *Acad. Emerg. Med.*, **2005**, *12*, 579-586.
- (4) Bernareggi, M.; Cremona, G. *Pulmonary Pharmacology & Therapeutics* **1999**, *12*, 331-352.
- (5) Yates, D.H. *Immunology and Cell Biology* **2001**, *79*, 178-190.
- (6) Zhang, X.; Broderick, M. *Mod. Asp. Immunobiol.* **2000**, *1*, 160-165.
- (7) Taha, Z. H. *Talanta* **2003**, *61*, 3-10.
- (8) Kojima, H.; Nakatsubo, N.; Kikuchi, K.; Kawahara S.; Kirino, Y.; Nagoshi H.; Hirata Y.; Nagano T. *Anal. Chem.* **1998**, *70*, 2446–2453.
- (9) Oh, B. D.; Stanton, A. C. *Appl. Optics* **1997**, *36*, 3294-3296.
- (10) Allen, B.; Piantadosi, C.; Ciury, L. *Nitric Oxide* **2000**, *4*, 75-84.
- (11) Malinski, T.; Taha, Z. *Nature* **1992**, *358*, 676-678.
- (12) Zhang, X.; Lin J.; Cardoso, L.; Broderick, M.; Darley-USmar, V. *Electroanalysis* **2002**, *14*, 697-703.

-
- (13) Zhang, X.; Lin J.; Cardoso, L.; Broderick, M.; Darley-USmar, V. *Electroanalysis* **2002**, *14*, 697-703.
- (14) Oh, B.D.; Stanton, A.C. *Applied Optics* **1997**, *36*, 3294-3296.
- (15) Roller, C. ; Namjou, K.; Jeffers, J. D.; Camp, M; Mock, A.; McCann, P. J.; Grego, J. *Applied Optics* **2002**, *41*, 6018-6029.
- (16) Binding, N.; Muller W.; Czeschinski, P. A.; Witting, U. *Eur. Respir. J* **2000**, *16*, 499-503.
- (17) Wada, M.; Morinaka, C.; Ikenaga, T.; Kuroda, N.; Nakashima, K. *Anal. Sci.* **2002**, *18*, 631.
- (18) Han, T.; Hyduke, D.; Vaughn, M., Fukuto, J., Liao, J. *Proc. Natl. Acad. Sci. USA* **2002**, *99*, 7763-7768.
- (19) Tamaki, J. *Materials Research Society Symposium Proceedings* **2005**, 828.
- (20) Iijima, S. *Nature* **1991**, *354*, 56-58.
- (21) Kong, J.; Franklin, N. R.; Zhou, C.; Chapline, M. G.; Peng, S.; Cho, K.; Dai, H. *Science* **2000**, *287*, 622-625.
- (22) Kong, J. ; Zhou, C.; Morpurgo, A.; Soh, H. T.; Quate, C. F; Markus, C.; Dai, H. *Appl. Phys.* **1999**, *69*, 305-308.
- (23) Qi, P.; Vermesh, O.; Grecu, M.; Javey, A.; Wang, Q.; Dai, H. *Nano Letters* **2003**, *3*, 347-351.
- (24) Star, A.; Han, T.; Joshi, V.; Gabriel, J.-C.P.; Gruener, G. *Adv.Mater.* **2004**, *16*, 2049-2052.
- (25) Star, A.; Joshi, V.; Thomas, D.; Niemann, J.; Gabriel, J.-C.P.; Valcke, C. *Nanotech.* **2005**, *5*, 104-107.

-
- (26) Qi, P.; Vermesh, O.; Grecu, M.; Javey, A.; Wang, Q.; Dai, H. *Nano Lett.* **2003**, *3*, 347-351.
- (27) Kong, J.; Franklin, N. R.; Zhou, C.; Chapline, M. G.; Peng, S.; Cho K.; Dai, H. *Science* **2000**, *287*, 622-625.
- (28) Star, A.; Joshi, V.; Skarupo, S.; Thomas, D.; Gabriel, J.-C. P. *J. Phys. Chem. B* **2006**, *110*, 21014-21020.
- (29) Star, A.; Han, T.-R.; Joshi, V.; Gabriel, J.-C. P.; Grüner, G. *Adv. Mater.* **2004**, *16*, 2049- 2052.
- (30) Kong, J.; Chapline, M.G.; Dai, H. *Adv. Mater.* **2001**, *13*, 1384-1386.
- (31) Lu, Y., Li, J.; Han, J.; Ng, H., Binder, C.; Partridge, C. M. *Chem. Phys. Lett.* **2004**, *391*, 344-346.
- (32) Someya, T.; Small, J.; Kim, P.; Nuckolls, C.; Yardley, J. *Nano Lett.* **2003**, *3*, 877-881.
- (33) Star, A.; Tu, E.; Niemann, J.; Gabriel, J.-C. P.; Joiner, C. S.; Valcke, C. *Proc. Natl. Acad. Sci. USA* **2006**, *103*, 921-926.
- (34) Shim, M.; Javey, K.; Kam, N. W. S.; Dai, H. *J. Am. Chem. Soc.* **2001**, *123*, 11512-11513.
- (35) Heinze, S.; Tersoff, J.; Martel, R., Derycke, V.; Apenzeller, J.; Avouris, Ph. *Phys. Rev. Lett.* **2002**, *89*, 106801-106804.
- (36) Kadish K. M. et al., *Porphyrin Handbook* Academic Press, New York **2000**.
- (37) Dolphin D., *The Porphyrins: Volume VII: Biochemistry, Part B*, Academic Press, New York **1979**.
- (38) Rakow, N. A.; Suslick, K. S. *Nature* **2000**, *406*, 710-713.

-
- (39) Morales-Bahnik, A.; Czolk, R.; Ache, H. J. *Sens. Actuators B* **1994**, 18-19, 493.
- (40) Czolk R. *Sens. and Actuator. B* **1996**, 30, 61-63.
- (41) Rodgers K. R. *Curr. Op. Chem. Bio.* **1999**, 3, 158-167.
- (42) Quintino, M. S. M.; Winnischofer, H.; Nakamura, M.; Araki, K.; Toma, H. E.; Angnes, L. *Anal. Chim. Acta* **2005**, 539, 215-222.
- (43) Ozoemena, K. I.; Zhao, Z.; Nyokong, T. *Electrochem. Commun.* **2005**, 7, 679-684.
- (44) Schwab, A. D.; Smith, D. E.; Bond-Watts, B.; Johnston, D. E.; Hone, J.; Johnson, A. T.; de Paula, J. C.; Smith, W. F. *Nano Lett.* **2004**, 4, 1261-1265.
- (45) Iijima S. *Nature* **1991**, 354, 56-58.
- (46) Avouris, P.; Appenzeller, J.; Martel, R.; Wind, S. J., *Proc. IEEE* **2003**, 91, 1772-1784.
- (47) Avouris P. *Acc. Chem. Res.* **2002**, 35, 1026-1034.
- (48) Merkoci, A.; Pumera, M.; Llopis, X.; Perez, B.; Valle, M.; Alegret, S. *Trends Anal. Chem.* **2005**, 24, 826-838.
- (49) Davis, J. J.; Coleman, K. S.; Azamian, B. R.; Bagshaw, C. B.; Green, M. L. H. *Chem. Eur. J.* **2003**, 9, 3732-3739.
- (50) Serp, P.; Corrias, M.; Kalck, P. *Appl. Catal. A* **2003**, 253, 337-358.
- (51) Belin, T.; Epron, F. *Mater. Sci. Eng. B* **2005**, 119, 105.
- (52) Jacquemin, R.; Kazaoui, S.; Yu, D.; Hassanien, A.; Minami, N.; Kataura, H.; Achiba, Y. *Synth. Met.* **2000**, 115, 283-287.
- (53) Kong, J.; Franklin, N. R.; Zhou, C.; Chapline, M. G.; Peng, S.; Cho, K.; Dai, H., *Science* **2000**, 287, 622.
- (54) Lee, C. Y.; Strano, M. S. *Langmuir* **2005**, 21, 5192-196.

-
- (55) Snow, E. S.; Perkins, F. K.; Robinson, J. A. *Chem. Soc. Rev.* **2006**, *35*, 790-798.
- (56) Guldi, D. M.; Rahman, G. M. A.; Jux, N.; Balbinot, D.; Hartnagel, U.; Tagmatarchis, N.; Prato, M. *J. Am. Chem. Soc.* **2005**, *127*, 9830-9838.
- (57) Murakami, H.; Nomura, T.; Nakashima, N. *Chem. Phys. Lett.* **2003**, *378*, 481-485.
- (58) Hasobe, T.; Fukuzumi, S.; Kamat, P. V. *J. Am. Chem. Soc.* **2005**, *127*, 11884-11885.
- (59) Hecht, D. S.; Ramirez, R. J. A.; Briman, M.; Artukovic, E.; Chichak, K. S.; Stoddart, J. F.; Grüner, G. *Nano Lett.* **2006**, *6*, 2031-2036.
- (60) Star, A.; Tu, E.; Niemann, J.; Gabriel, J. C. P.; Joiner, C. S.; Valcke, C. *Proc. Natl. Acad. Sci. USA* **2006**, *103*, 921.
- (61) Jeng, E. S.; Moll, A. E.; Roy, A. C.; Gastala, J. B.; Strano, M. S. *Nano Lett.* **2006**, *6*, 371.
- (62) Heller, D. A.; Jeng, E. S.; Yeung, T. K.; Martinez, B. M.; Moll, A.E.; Gastala, J. B.; Strano, M. S. *Science* **2006**, *311*, 508-511.
- (63) Kataura, H.; Kumazawa, Y.; Maniwa, Y.; Umezumi, I.; Suzuki, S.; Ohtsuka, Y.; Achiba, Y. *Synth. Met.* **1999**, *103*, 2555-2558.
- (64) Bachilo, S. M.; Strano, M. S.; Kittrell, C.; Hauge, R. H.; Smalley, R. E.; Weisman, R. B. *Science* **2002**, *298*, 2361-2366.
- (65) Aihara J. *J. Phys. Chem. A* **1999**, *103*, 7487-7495.
- (66) Jortner, M.; Ratner, M. *Molecular Electronics*, Blackwell Science, Malden, MA, USA **1997**.
- (67) Schreiber F. *Prog. Surf. Sci.* **2000**, *65*, 151-256.
- (68) Filler, M. A.; Bent, S. F. *Prog. Surf. Sci.* **2003**, *73*, 1-56.

-
- (69) Lee, J.-G.; Ahner, J.; Yates J.T. Jr., *J. Am. Chem. Soc.* **2002**, *124*, 2772-2780.
- (70) Lee, J.-G.; Ahner, J.; Yates J.T. Jr. *J. Chem. Phys.* **2001**, *114*, 1414-1419.
- (71) Poulston, S.; Bennett, R. A.; Jones, A. H.; Bowker, M. *Phys.Rev. B* **1997**, *55*, 12888-12891.
- (72) Poulston, S.; Bennett, R. A.; Jones, A. H.; Bowker, M. *Surf. Sci.* **1997**, *377*, 66.
- (73) Aas, N.; Bowker, M. J. *Chem. Soc. Faraday Trans.* **1993**, *89*, 1249.
- (74) Frederick, B.G.; Ashton, M.R.; Richardson, N.V.; Jones, T.S. *Surf. Sci.* *292*, **1993**, 33-35.
- (75) Lee J.-G.; Ahner J.; Mocuta D.; Denev S.; Yates J.T. Jr. *J. Chem. Phys.* **2000**, *112*, 3351-3356.
- (76) Hasselstrom, J.; Karis, O. ; Weinelt, M. ; Wassdahl, N.; Nilsson, A.; Nyberg, M ; Pettersson, L.G.M. ; Sammant, M.G; Stohr, J. *Surf. Sci.* **1998**, *407*, 221-224.
- (77) Bitzer, T.; Richardson, N.V.; Reiss, S.; Wuhn, M.; Woll, C. *Surf. Sci.* **2000**, *458*, 173-178.
- (78) Chen, Q.; Perry, C.C.; Frederick, B.G.; Murray, P.W.; Haq, S.; Richardson N.V. *Surf. Sci.* **2000**, *446*, 63-75.
- (79) Bitzer, T.; Richardson N.V. *Surf. Sci.* **1999**, *428*, 369-373.
- (80) Frederick, B.G. ; Chen, Q.; Leibsle, F.M.; Lee, M.B.; Kitching, K.J.; Richardson, N.V. *Surf. Sci.* **1997**, *394*, 1-25.
- (81) Frederick, B.G.; Leibsle, F.M.; Haq, S.; Richardson, N.V. *Surf. Rev. Lett.* **1996**, *3*, 1523-1546.
- (82) Pudney, P.D.A.; Frederick, B.G.; Richardson, N.V. *Surf.Sci.* **1994**, *309*, 46-51.
- (83) Neuber, M.; Zharnikov, M.; Walz, J.; Grunze, M. *Surf.Rev. Lett.* **1999**, *6*, 53-75.

-
- (84) Guo, Q.; Cocks, I.; Williams, E. M. *Surf. Sci.* **1997**, *393*, 1-11.
- (85) Bitzer, T.; Richardson, N. V. *Surf. Sci.* **1999**, *427*, 369-373.
- (86) Ahner, J.; Mocuta, D.; Yates J.T. Jr. *J. Vac. Sci. Technol. A* **1999**, *17*, 2333-2338.
- (87) Thompson, L.; Lee, J.-G.; Maksymovych P.; Ahner, J.; Yates J. T. Jr. *J. Vac. Sci. Technol. A* **2003**, *21*, 491-494.
- (88) Weast R.C.; Astle, M.J.; Beyer, W.H. CRC Handbook of Chemistry and Physics, CRC Press, Inc., Boca Raton, Florida **1988**.
- (89) Karis, O.; Hasselstrom. J.; Wassdahl N.; Weinelt, M.; Nilsson, A.; Nyberg, M.; Pettersson, L. G. M.; Stohr, J.; Samant M.G. *J. Chem. Phys.* **2000**, *112*, 8146-8155.
- (90) Bowker, M.; Madix, R. J. *Surf. Sci.* **1981**, *102*, 542-553.
- (91) Bowker, M.; Madix, R. J. *Appl. Surf. Sci.* **1981**, *8*, 299-309.
- (92) Surman, M.; Lackey, D.; King, D. A. *J. Electron Spectrosc.Relat. Phenom.*, **1986**, *39*, 245-250.
- (93) Gao, Q.; Cheng, C. C.; Chen, P. J.; Choyke, W. J.; Yates J. T. Jr. *J. Chem. Phys.*, **1993**, *98*, 8303-8311.
- (94) Miskovic, Z.; Vukanic, J.; Madey, T. E. *Surf. Sci.* **1984**, *141*, 285-291.
- (95) Miskovic, Z.; Vukanic, J.; Madey, T. E. *Surf. Sci.* **1986**, *169*, 405-412.